Vibration-induced friction modulation for a general frequency of excitation

Sulollari, E.; van Dalen, K.N.; Cabboi, A.

DOI
10.1016/j.jsv.2023.118200

Publication date
2023

Document Version
Final published version

Published in
Journal of Sound and Vibration

Journal of Sound and Vibration 573 (2024) 118200

Contents lists available at ScienceDirect

Journal of Sound and Vibration

journal homepage: www.elsevier.com/locate/jsvi

Vibration-induced friction modulation for a general frequency of excitation

E. Sulollari *, K.N. van Dalen, A. Cabboi

Department of Engineering Structures, Faculty of Civil Engineering and GeoSciences, Delft University of Technology, Stevinweg 1, 2628CN Delft, Netherlands

ARTICLE INFO

Keywords:
Average friction
Mechanical vibration
Stick–slip
Vibrorheology
Method of direct separation of motion

ABSTRACT

Applying an oscillatory load is one of the most efficient ways to alter friction forces. Several theoretical and experimental studies on the influence of oscillatory loads on friction have been conducted, investigating the effect of both in-plane and out-of-plane oscillations for different tribological pairings. However, in the literature, the effect of an oscillatory load on the friction force has been studied with an emphasis on dynamic loads characterized by a high-frequency content, while a clear statement as to what is considered "high-frequency" is missing. Moreover, the effect of a combination of load directions on the friction reduction is not accounted for. Therefore, this study aims to determine the vibration-induced effect on friction regardless of the frequency range and direction of harmonic force for a single and multi-degree-of-freedom system. Analytical methods are used to obtain the friction modulation due to harmonic loads, considering a classical mass–spring–dashpot system on a moving belt and the Amontons–Coulomb law. It is found that, in the case of continuous slip, a general relation for the vibration-induced friction modulation is obtained utilizing the velocity response function of the investigated system. The latter is used to highlight a threshold from which the high-frequency regime starts and to determine the stick–slip boundaries. Moreover, through the velocity response function, the influence of different external harmonic forces is investigated and discussed. This includes considerations of phase, excitation frequency, system characteristics, and the choice of the normal contact force expression.

1. Introduction

Friction control is crucial for the satisfactory operation of systems in many fields of applied science. Lubricants are commonly used as a way to control and reduce friction between surfaces in contact, improving their performance and adding value in terms of cost savings and expenses that arise due to wear and tear, repair, and maintenance of parts in contact. However, timely lubrication is required to ensure the proper functioning of tools, automotive and machines, and the removal and replacement (if needed) of the lubricant can be a quite challenging task. Exploiting the effects induced by a deliberately applied oscillatory force is another method used to alter friction forces. This is a flexible alternative that can be considered as a form of lubrication that can be controlled and removed very quickly by changing the amplitude and the frequency of the oscillatory force. Examples of applications in which a vibration-assisted technique is used to alter friction can be found for positioning control in robots [1], decommissioning of joints [2], pile driving [3], needle insertions [4] and drilling operations [5]. Ultrasonic oscillations, for example, are used to alter friction in wire drawing and cutting, metal working [6], in nanotribological devices by means of atomic force microscopes [7], for rendering

* Corresponding author.
E-mail addresses: E.Sulollari@tudelft.nl (E. Sulollari), K.N.vanDalen@tudelft.nl (K.N. van Dalen), A.Cabboi@tudelft.nl (A. Cabboi).

https://doi.org/10.1016/j.jsv.2023.118200
Received 3 June 2023; Received in revised form 10 November 2023; Accepted 5 December 2023
Available online 7 December 2023

texture on haptic surfaces [8] and in friction stir welding [9]. However, despite the technique successfully being used for specific applications, a universally accepted physical interpretation of how static and kinetic friction forces change and react to externally applied excitation is still missing. This is mainly due to the absence of a universal law friction and the missing link between surface property variation and external applied forces, but also because most of the current applications are specifically focused on the use of applied oscillatory forces characterized by a high-frequency content.

The fact that friction forces can be significantly reduced by applying external excitation has been known since at least the 1950s [10,11]. In the '60s and '70s, most of the experimental results obtained seem to be strongly dependent on the characteristics of each test rig. Thus, no general law explaining the observed behavior was identified. Since then, several experimental and theoretical studies have been conducted to understand the effect of an external excitation on friction and exploit it in practical applications. At the beginning of the '90s, analytical and numerical attempts were made by Hess and Soom [12–14]. Their studies showed that normal oscillations applied on top of a Hertzian and adhesion-like contact lead to a reduction of contact deflection and consequently of the average area of contact and the average friction force. Matunaga and Onoda [15] investigated the effect of vibration on friction on a mass sliding on an in-plane vibrating table. To illustrate the mechanism of friction reduction by means of vibration, they proposed the concept of effective, time-averaged frictional forces. Based on this concept, Storck and coworkers [16] and Kumar and Hutchings [17] studied the reduction of the friction force due to ultrasonic vibrations applied parallel and perpendicularly to the sliding direction. For each loading case, qualitative good matches between theoretical predictions and measurements were obtained. These studies assume the Amontons–Coulomb's law and the friction force varies due to the change of direction of the resultant sliding velocity vector. Hence, the "friction reduction" results from the average frictional force over a whole vibration cycle. Later on, Leus and Gutowski [18] showed that using the Dahl model [19], in which asperities are modeled by means of micro-springs characterized by a shear stiffness, the above-mentioned averaged friction force could be reduced independently of whether a change in the direction of the net friction force vector is observed. Grudzinski and Kostek [20] also considered the surfaces in friction contact to be rough, creating an elastic interface modeled by non-linear springs. In this model, the external force applied was a constant one instead of an harmonic one. The study showed that the main cause of the decrease in the friction force could be due to complex non-linear dynamic processes occurring at the asperity level. Popov and coworkers [21–23] also studied the effect of ultrasonic oscillations on the averaged friction force, both experimentally and theoretically, considering in-plane and out-of-plane oscillatory excitation separately and different tribological pairings [21]. By assuming the Amontons–Coulomb's friction law, the measurements of friction coefficients vs sliding velocity for different amplitudes of the oscillation velocity fitted well with theoretical predictions for sliding velocities larger than the actuation velocity. For small sliding velocities, the measured friction coefficient tends to a finite value, contradicting theoretical results that predict the averaged friction force to approach zero as sliding velocity goes to zero [21]. To explain the latter discrepancy, Popov and his coworkers stressed out the relevance of introducing a tangential contact stiffness and any interface dynamic process in the model [24,25].

In parallel to the aforementioned works from the friction research community, studies originating from the structural dynamic community also focused on the interaction between the global dynamics of the system and the vibration-induced friction reduction. These studies explored a different computational route to friction reduction. For example, in the research conducted by Thomsen [26], the Method of Direct Separation of Motion (MDSM) was used (see [27] for more details on the MDSM). The main idea of MDSM lies in separating the motion of a dynamic system arising due to high-frequency excitation into two components of motion, a "slow" and a "fast" one. The slow component is usually of primary interest and equations describing it are simpler than the initial equations. Approximations are involved only for solving the equations of fast motion and do not strongly affect the accuracy of the resulting equations for the slow motion, because only averaged fast components are employed in their formulation [28]. In 2014, Sorokin [29] suggested a modification of the MDSM. This version of the MDSM allows for solving a broader range of problems, namely problems that do not imply restrictions on the spectrum of excitation frequencies. In problems with friction, MDSM has been applied in cases of harmonic excitation of small amplitude and very high frequency only. Michaux and coworkers [30], for example, investigated the effect of the waveform of different periodic signals on the effectiveness of tangential high-frequency excitation to cancel friction-induced oscillation using a single-degree-of-freedoms system. Hoffmann and coworkers [31] also used the MDSM to quench mode-coupling friction-induced instability using high frequency in a 2-degree of freedom system. In more recent works [32,33], the effects of longitudinal high-frequency excitation on contact compliance considering different dynamic friction models were studied, performing analytical, numerical and experimental investigations.

In both research communities described above, the effect of external load on friction force has been studied with an emphasis on loads characterized by a high-frequency content (i.e. ultrasonic vibration over 20 kHz). However, in the literature, a clear statement as to what is considered "high-frequency" with reference to vibration-induced friction modulation is still missing. Blekhman [28] provided a rule of thumb for applied problems, indicating that an excitation frequency around 3–5 times the natural frequency could be considered as high frequency, without showing any explicit demonstration. Moreover, the applied load directions in all the aforementioned studies is either normal or tangential to the sliding direction. The effect of a combination of load directions on the friction behavior is also missing. Lastly, the nature of the normal contact force (stiffness or inertia driven) and how the tangential friction force depends on it is also seldomly discussed. Therefore, the first aim of this study illustrated in Section 2 aims at extending the existing investigations on the effect of a high-frequency harmonic load to friction to a general excitation frequency range and defining a threshold starting from which a high-frequency regime can be identified. For this purpose, the MDSM will be extended considering initially a single load case. In the same section, the second aim is to unify and explain the similar results in terms of friction reduction due to vibrations (only with reference to the Amontons–Coulomb's friction law) obtained by both the aforementioned research communities, even though different methods were used from both sides (without ever cross-referencing each other). To bridge this gap, it will be shown that the underlying physical mechanism of friction reduction due to vibration resides

in the velocity response function of the dynamic system. Moreover, while in some studies it is mentioned that the effect of excitation on sliding friction is investigated, none of these works (with the exception of Teidelts and Mao's studies, see [23,25], respectively) distinguish the presence of the stick–slip and sliding regimes. To compute vibration-induced friction reduction, however, it is important to know whether the system is stick–slipping or not. Thus, in Section 3, it is pointed out that in order to get analytical solutions for the vibration-assisted friction modulation, the analysis has to be framed with reference to the identification of stick–slip boundaries. To such regard, it is shown that the velocity response function is not only crucial to compute the friction modulation due to vibration, but it also provides a more intuitive insight to the identification of the stick–slip regime, compared to the analysis shown in other seminal works on such topics [34–36]. Besides the extension to a general frequency of excitation, in Section 4 the vibration-assisted friction reduction is also investigated for a two degree of freedom system, assessing the influence of different harmonic load combinations: tangential and normal ones with reference to contact surface. Lastly, the effect of introducing a different expression of the normal contact force, dependent either on the contact stiffness and damping or on the inertial force, is investigated and its consequences on the vibration-assisted friction reduction are discussed.

2. Method of direct separation of motion for a forced single-degree-of-freedom system

In this section, a single-degree-of-freedom system will be considered to investigate the effect of external excitation on the friction force. At first, the method of direct separation of motion is illustrated to quantify such effect, limited to the case of high-frequency excitation. The vibration-induced friction reduction results are then compared with the ones obtained using alternative methods available in the literature. Lastly, the MDSM will be extended to include the effect of a general frequency of excitation.

2.1. Illustrative example of the method of direct separation of motion for high-frequency excitation

To illustrate the procedure of applying the MDSM, the single-degree-of-freedom system (SDOF) characterized by a mass–spring–damper configuration in contact with a moving belt is considered, as shown in Fig. 1. The non-dimensional equation of motion for this system is

$$\ddot{x} + 2\beta\dot{x} + x + \gamma^2\mu_s \mathrm{sgn}(v_r) = \alpha\Omega^2 \sin(\Omega\tau) \tag{1}$$

where $\dot{x} = \frac{dx}{d\tau}$ is the non-dimensional velocity of the mass at non-dimensional time τ, μ_s is the coefficient of static friction and

$$\tau = \omega_n t, \quad \omega_n^2 = \frac{K}{M}, \quad x = \frac{X}{L}, \quad 2\beta = \frac{C}{\sqrt{KM}}, \quad \gamma^2 = \frac{g/L}{K/M}, \quad \Omega = \frac{\Omega_e}{\omega_n}, \quad \alpha = \frac{mr}{ML}, \quad v_r = \dot{x} - v_b, \quad v_b = \frac{V_b}{\omega_n L}. \tag{2}$$

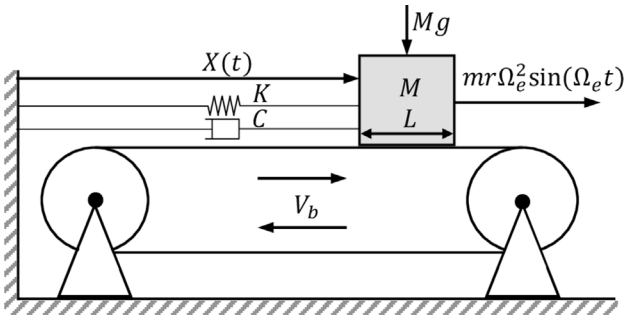

Fig. 1. Mass–spring–damper system on a moving belt, subject to a friction force and applied harmonic loading.

For the chosen model setup, we consider the kinetic friction to be the same as the static friction. The adopted friction law for this illustrative example is the Amontons–Coulomb's law. Throughout the paper, the following formulation is used

$$\mu(v_r) = \mu_s \mathrm{sgn}(v_r). \tag{3}$$

which defines the friction coefficient as a function of the relative velocity's sign. To clarify the parameters in Eq. (2), the belt's motion is represented by the speed V_b, the mass M is a rigid body with a characteristic length L and position $X(t)$ at time t, subjected to gravity loading Mg, a linear spring force KX, a damping force $C\mathrm{d}X/\mathrm{d}t$ and a friction force $Mg\mu(V_r)$. Time is normalized by the natural frequency ω_n of the undamped system. The damping ratio is described by β and γ^2 defines the ratio between the gravity force and the spring force. Parameters v_b, Ω and α represent the non-dimensional speed of the belt, the non-dimensional frequency of harmonic excitation and the non-dimensional amplitude of excitation, respectively. The SDOF system is forced by a time-harmonic loading, characterized by a frequency Ω_e and an amplitude $mr\Omega_e^2$ (e.g., load arising from a horizontally unbalanced mass m at eccentricity r [26]).

In previous works [26,27], it was shown that if the external forcing is characterized by a high-frequency oscillation and by a small amplitude ($\Omega \gg 1$ and $\alpha \ll 1$, respectively), the MDSM allows to quantify the reduction of the friction force, averaged over

one vibration cycle, governed by the high-frequency excitation. To do so, the MDSM separates the motion $x(\tau)$ into its slow and fast components as follows

$$x(\tau) = z(\tau) + \Omega^{-1}\phi(\tau, \Omega\tau) \tag{4}$$

where $z(\tau)$ describes the slow motion at the time scale of free oscillation of the given SDOF system, and ϕ describes the fast motion at the rate of the external excitation. Thus, τ represents the slow time scale whereas $\Omega\tau$ defines the fast time scale. Note that these time scales are considered independent. Typically, for engineering applications (e.g. see [3]), the effects induced by the fast motion ϕ on the motion z would be of primary interest. As discussed in [27], to make the transformation of variables from x to z and ϕ unique, the following constraint is necessary

$$\langle \phi(\tau, \Omega\tau) \rangle = \frac{1}{2\pi} \int_0^{2\pi} \phi(\tau, \Omega\tau) \mathrm{d}(\Omega\tau) = 0 \tag{5}$$

where $\langle\rangle$ defines the average operator over the period of the rapidly oscillating component. The transformation of variables is carried out by substituting Eq. (4) into Eq. (1), and imposing the constraint given by Eq. (5). The resulting expression reads as follows

$$\ddot{z} + 2\beta\dot{z} + z + \gamma^2 \left\langle \mu(\dot{z} + \phi' + \Omega^{-1}\dot{\phi} - v_b) \right\rangle = 0 \tag{6}$$

where $\dot{z} = \frac{\mathrm{d}z}{\mathrm{d}\tau}$, $\dot{\phi} = \frac{\partial\phi}{\partial\tau}$, and $\phi' = \frac{\partial\phi}{\partial(\Omega\tau)}$.

Since the purpose of this example is to quantify the effect of the external forcing on the friction force, the expression representative of the fast motion ϕ should be retained. As shown in [26,27], to isolate the fast motion, the equation of slow motion z shown in Eq. (6) is subtracted from the main governing equation defined by Eq. (1), resulting in

$$\Omega\phi'' + 2\dot{\phi}' + \Omega^{-1}\ddot{\phi} + 2\beta(\phi' + \Omega^{-1}\dot{\phi}) + \Omega^{-1}\phi + \gamma^2 \left(\mu(\dot{z} + \phi' + \Omega^{-1}\dot{\phi} - v_b) - \left\langle \mu(\dot{z} + \phi' + \Omega^{-1}\dot{\phi} - v_b) \right\rangle \right) = \alpha\Omega^2 \sin(\Omega\tau). \tag{7}$$

At this stage, it is important to anticipate that when using Amontons–Coulomb's law and in the absence of any stick regime, meaning that $\dot{x} \neq v_b$ ($v_r \neq 0$), the average $\langle \mu(v_r) \rangle$ is equal to μ_s. In this case, Eqs. (6)–(7) are simplified to

$$\ddot{z} + 2\beta\dot{z} + z + \gamma^2\mu_s = 0, \tag{8}$$

and

$$\Omega\phi'' + 2\dot{\phi}' + \Omega^{-1}\ddot{\phi} + 2\beta(\phi' + \Omega^{-1}\dot{\phi}) + \Omega^{-1}\phi = \alpha\Omega^2 \sin(\Omega\tau). \tag{9}$$

The solutions of Eqs. (8) and (9) each have a transient and a steady-state response. At steady-state motion, the displacement response of the motion z is just a constant, meaning its velocity response will be zero. Since sinusoidal forcing is present on the right-hand side of Eq. (9), the displacement and velocity response in the steady state will be harmonic. Thus, only the solution of ϕ contributes to the steady-state velocity response. In Section 2.3, a more detailed discussion concerning the link between the transient/steady-state solutions and the fast/slow components of motion will be provided.

To isolate the high-frequency vibration-induced effect on friction, we exploit the underlying assumption that $\Omega \gg 1$, meaning that all the terms in Eq. (7) multiplied by Ω^{-1} and Ω^{-2} are small, and the equation of the fast motion can be expressed in the following compact form

$$\phi'' = \alpha\Omega \sin(\Omega\tau) + O(\Omega^{-1}) + O(\Omega^{-2}) \tag{10}$$

where $O(\Omega^{-1})$ and $O(\Omega^{-2})$ denote terms significantly smaller than 1. The solution of fast motion ϕ and its corresponding derivative ϕ' are

$$\phi = -\alpha\Omega \sin(\Omega\tau) \quad \text{and} \quad \phi'(\tau, \Omega\tau) = -\alpha\Omega \cos(\Omega\tau). \tag{11}$$

Hence, substituting this solution into the equation of the slow motion given by Eq. (6) results in

$$\ddot{z} + 2\beta\dot{z} + z + \gamma^2 \langle \mu(\dot{z} - \alpha\Omega \cos(\Omega\tau) - v_b) \rangle = 0. \tag{12}$$

The following term from Eq. (12)

$$\bar{\mu} = \langle \mu(\dot{z} - v_b - \alpha\Omega \cos(\Omega\tau)) \rangle \tag{13}$$

enables to quantify the vibration-induced effect on friction. Therefore, the term "effective friction" is used for $\bar{\mu}$. In this study, the expression of the effective friction force is obtained for steady-state vibratory motion only. Thus, no information is provided for the vibration-induced effect on friction during the transient response. Since steady-state motion is considered, there is no contribution due to $\dot{z}$, so the expression of relative velocity, $\dot{z} - v_b$, reduces to $-v_b$. Since the continuous-sliding regime is assumed, it should be checked that for each v_b value considered, the system remains in the sliding regime.

In case of interest, the slow motion z can be found by solving Eq. (12). However, to study the effect induced by the high-frequency excitation on the averaged friction force, it is sufficient to evaluate $\bar{\mu}(v_b)$. It is worth highlighting that the effective friction expression defined in Eq. (13) holds for any constitutive law of friction characterized by a dependence on the relative velocity. Dynamic friction laws of the rate-and-state types [37,38] were not tested so far. On such regards, the reader might be interested in [32],

where numerical solutions were provided for Eq. (13), while accounting for an elasto-plastic friction law. With reference to the Amontons–Coulomb's law defined in Eq. (3), the effective friction expression reads as follows

$$\bar{\mu}(v_b) = \langle \mu(-v_b - \alpha\Omega\cos(\Omega\tau))\rangle = \mu_s \langle \mathrm{sgn}(-v_b - \alpha\Omega\cos(\Omega\tau))\rangle\,, \tag{14}$$

$$\bar{\mu}(v_b) = \begin{cases} \mu_s(1 - \frac{2}{\pi}\arccos(-\frac{v_b}{\alpha\Omega})) & \text{for } |v_b| \le \alpha\Omega \\ \mu_s \mathrm{sgn}(-v_b) & \text{for } |v_b| \ge \alpha\Omega. \end{cases} \tag{15}$$

Fig. 2 shows the effective friction defined by Eq. (15) as a function of the belt velocity v_b. It should be noted that, while negative signs are present in Eq. (14), suggesting negative friction values for positive belt velocities, the plot follows an opposite sign convention, to be comparable and in line with other studies on such topic (see [16,17,26]). The black dashed lines in Fig. 2 mark the following equality $v_{b,c} = \alpha\Omega$. The index c refers to the value of v_b from which the effective friction coefficient becomes the constant μ_s again. Two conclusions can be drawn by inspecting the $\bar{\mu}(v_b)$ vs. v_b graph. First, for $|v_b| \le \alpha\Omega$, the typical discontinuity of the coefficient of friction observed at $v_b = 0$ is smoothed, since the effective friction expression is characterized by a shape governed by the arc-cosine function. Secondly, for $|v_b| > \alpha\Omega$, the effective friction characteristic $\bar{\mu}(v_b)$ equals μ_s which is the friction value for the case of $\alpha\Omega = 0$. In other words, no effect on the averaged friction force due to the high-frequency excitation is observed.

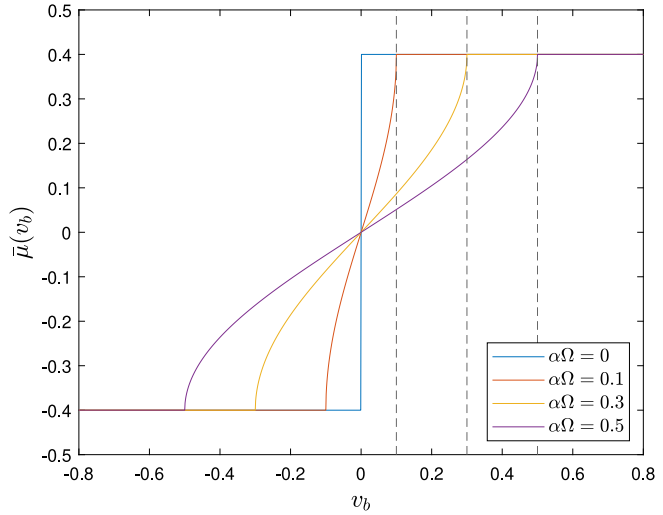

Fig. 2. Effective friction $\bar{\mu}(v_b)$ behavior as given by Eq. (15) for different values of $\alpha\Omega$.

In the next subsection, the method is compared to an alternative one used to obtain the effective friction under high-frequency excitation. Comparing the MDSM with the alternative method will allow to unify and explain the similar results in terms of friction reduction obtained by different research communities, even though different approaches were used from each side.

2.2. Alternative methods for high-frequency excitation

In the literature, alternative models exist that predict the effect of excitation on friction. Studies by [15–17] were devoted to giving an explanation to the friction force reduction when ultrasonic vibrations were superimposed to macroscopic motion. The ultrasonic excitation was applied either parallel or perpendicular to the sliding direction. The reduction on friction was analyzed both experimentally as well as theoretically, and for the latter Amontons–Coulomb's law was considered.

Fig. 3(a) shows the model considered by [16,17], with the excitation applied parallel to the sliding direction. Body A is assumed to slide with a constant velocity V_b over body B which has an oscillatory motion of amplitude α and angular frequency Ω_e along the same line of action as that of V_b. When the instantaneous velocity of B, $V(t)$, is greater than V_b, the friction force on body A, F_f, will reverse its direction and act in the same direction as V_b. In Fig. 3(b) the corresponding variation of the frictional force with time over one cycle is shown. The friction force, F_f, first changes from positive to negative and then to positive again (interval OC, CD and DG, respectively). The time t_b taken for the vibration velocity to reach the sliding velocity V_b is given by

$$t_b = \frac{1}{\Omega_e}\sin^{-1}\left(\frac{V_b}{\alpha\Omega_e}\right). \tag{16}$$

The time CD for which the friction force is negative is equal to the time EF over which it is positive. While averaging over one cycle, these two will cancel each other out. The resultant average frictional force over the whole cycle F_a is thus given by

$$F_a = \frac{F_f}{T}4t_b = F_f\frac{2}{\pi}\sin^{-1}\left(\frac{V_b}{\alpha\Omega_e}\right). \tag{17}$$

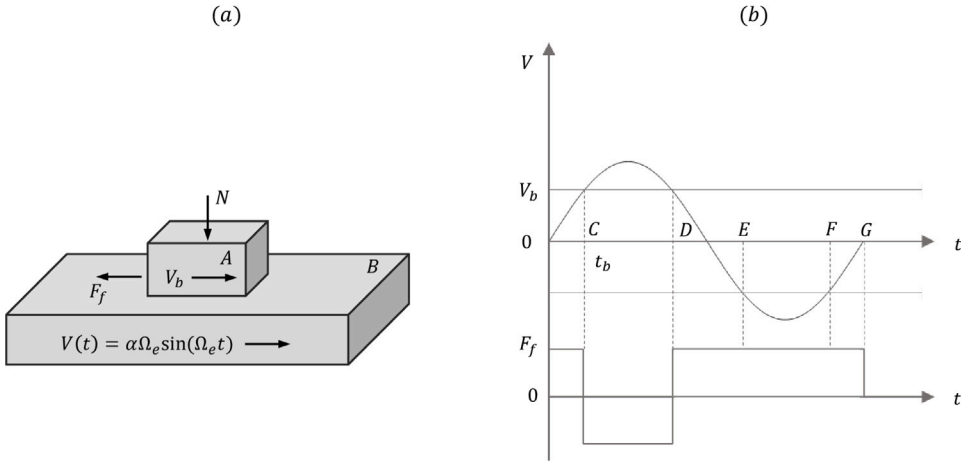

Fig. 3. (a) The model considered for sliding motion and subjected to an excitation along the sliding direction; (b) Variation of vibration velocity with time and the corresponding change in direction of frictional force.

where $T = \frac{2\pi}{\Omega_e}$ is the period of vibration.

Eq. (17) is valid only for $\alpha\Omega_e > V_b$, so the amplitude of the velocity of body B should be bigger than the constant velocity V_b. If the sliding velocity V_b is higher, Eq. (17) ceases to apply because, in that case, the friction force opposes the direction of macroscopic sliding during the whole duration of a cycle of vibration. Since the friction force does not change direction, no reduction in friction is predicted. Considering the friction force, $F_f = \mu_s N$, and the constant sliding velocity V_b to be either positive or negative, the effective friction under the effect of ultrasonic oscillation can be written as

$$\mu_a = \begin{cases} \mu_s \frac{2}{\pi} \sin^{-1}\left(\frac{V_b}{\alpha\Omega_e}\right) & \text{for } |V_b| \le \alpha\Omega_e \\ \mu_s \text{sgn}(V_b) & \text{for } |V_b| \ge \alpha\Omega_e. \end{cases} \tag{18}$$

where $\mu_a = F_a/N$.

Eq. (18) portrays the effect of ultrasonic oscillations on the friction force, thus, it should be possible to compare it with the effective friction expression obtained in Eq. (15). Firstly, it is important to realize that the constant belt velocity v_b and the excitation frequency Ω used in Section 2.1 are non-dimensional terms. Thus, for $\omega_n = 1$ and $L = 1$, v_b and Ω correspond to V_b and Ω_e (see Eq. (2)), respectively. From both expressions (Eqs. (15) and (18)), it is inferred that for belt velocities higher than the amplitude of the oscillation velocity, no change in friction force is observed. To compare the equations for belt velocities lower than $\alpha\Omega_e$, both expressions are plotted in Fig. 4 for $\alpha\Omega_e = 0.3$. From the figure, it is observed that the plots coincide, proving that both methods give the same results.

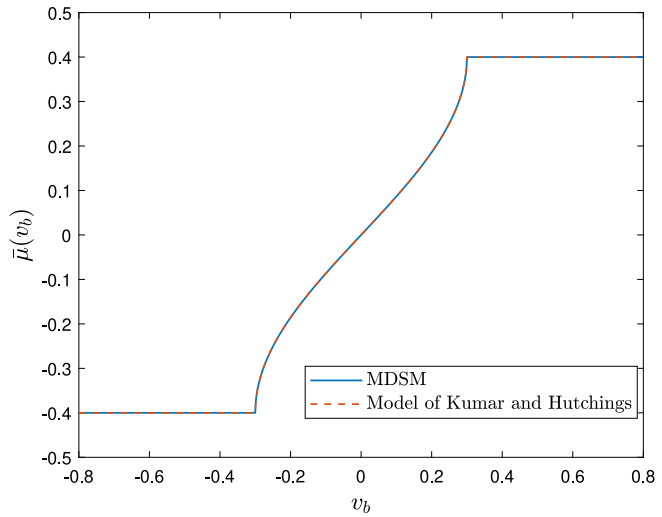

Fig. 4. Comparison of $\bar{\mu}(v_b)$ obtained using MDSM and the model of [17].

It is worth highlighting again that these results (using MDSM and by [17]) are reached considering steady-state vibratory motion within a continuous-sliding regime. For certain combinations of belt velocity, excitation amplitude and frequency, stick–slip might

occur, making the analytical expressions of the effective friction force invalid. However, none of the studies explicitly mention such limitation. Moreover, while it is possible to straightforwardly get the effective friction force using the rationale depicted in Fig. 3, see also [16,17], this model gives the same results as the MDSM for the case of Amontons–Coulomb's law and high-frequency vibration. If another friction law or a general frequency of excitation is considered, it becomes hard or even impossible to obtain the effective friction characteristic with this approach. Moreover, the MDSM is more versatile, since it can be applied to systems with more than just one degree of freedom.

The rationale depicted in [16,17] was also used to evaluate a friction change considering the Dahl model, see [18], which accounts for the asperity's compliance along the sliding direction. To solve for this model however, a numerical procedure was implemented and the friction force reduction was calculated over one period of oscillation. While in the case of the Amontons–Coulomb's law, the change in friction force direction occur instantaneously, Fig. 3(b), when using the Dahl model, the change of friction force direction is not abrupt and depends on the value of the tangential contact stiffness. In the latter model, like [16,17], a friction reduction was observed only for $V_b < \alpha\Omega_e$. As the value of the tangential contact stiffness increases, the Dahl model reduces to Eq. (18).

2.3. Extension of the MDSM for a general frequency of excitation

In Sections 2.1–2.2, the effect of high-frequency excitation on friction was presented. To seek a more general expression able to quantify the vibration-induced effect on friction, the following subsection aims at extending the MDSM procedure illustrated above to a general frequency of excitation of the system. A modification of the MDSM aiming at relaxing the restriction on the spectrum of excitation frequencies was already proposed in previous studies [28,29]. However, its application to a friction-driven system has never been investigated. To illustrate the procedure, the system shown in Fig. 1 is considered again. As already discussed in Section 2.1, to compute the effective friction expression, the equation for the fast motion ϕ, Eq. (7), is needed.

In Section 2.1, since $\Omega \gg 1$, all the terms multiplied by Ω^{-1} and Ω^{-2} were small terms and could be ignored. To find the effect caused on the averaged friction force by a general frequency of excitation, the condition $\Omega \gg 1$ does not hold anymore, meaning that all the terms in Eq. (7) should be retained. It is worth highlighting that the assumption $\Omega \gg 1$ is relevant if the interest resides in computing the effect of excitation on the slow motion term $z(\tau)$. However, if the interest lies only in computing an averaged friction force reduction during a steady-state oscillatory motion, an analytical expression of the friction reduction can be obtained for a general harmonic forcing.

To solve Eq. (7), the rationale used in [28,29] is adopted. It is worth highlighting that the extension of the MDSM to a general harmonic forcing presented in this section differs from the one shown in [28,29], as it considers the original MDSM. The solution is sought in form of a harmonic series by means of the method of varying amplitude (MVA) proposed in [39] and also applied in [28,29]. A possible harmonic series solution is

$$\phi = B_{11}(\tau)\sin(\Omega\tau) + B_{12}(\tau)\cos(\Omega\tau) + B_{21}(\tau)\sin(2\Omega\tau) + B_{22}(\tau)\cos(2\Omega\tau) + \cdots \tag{19}$$

In the leading-order approximation, only the first two terms are needed, resulting in

$$\phi = B_{11}(\tau)\sin(\Omega\tau) + B_{12}(\tau)\cos(\Omega\tau). \tag{20}$$

Note that as continuous sliding is considered and no nonlinearities are present in the system, Eq. (20) provides the closed-form solution. Moreover, the time-scale τ of the varying amplitude of the B_{11} and B_{12} parameters do not need to vary slowly with reference to the time-scale of the sinusoidal function $\Omega\tau$, as discussed in [39].

Inserting Eq. (20) into Eq. (7), and gathering the coefficients of the involved harmonics $\sin(\Omega\tau)$, $\cos(\Omega\tau)$, results in one expression for $\ddot{B}_{11}$ and one for $\ddot{B}_{12}$. Using some cumbersome mathematical manipulations, the solution for ϕ in Eq. (7) can be obtained analytically. Both $B_{11}(\tau)$ and $B_{12}(\tau)$ approach to a constant value as τ increases, thus reaching a steady-state condition. At steady state, $B_{11}(\tau)$ and $B_{12}(\tau)$ are described by

$$B_{11} = -\frac{\alpha\Omega^3(\Omega^2-1)}{(4\beta^2-2)\Omega^2+1+\Omega^4}, \quad B_{12} = -\frac{2\beta\alpha\Omega^4}{(4\beta^2-2)\Omega^2+1+\Omega^4}. \tag{21}$$

Using these expressions for B_{11} and B_{12}, the solution in terms of ϕ in the steady state (same symbol used for notational brevity) becomes

$$\phi = \frac{\alpha\Omega^3}{\sqrt{4\beta^2\Omega^2+(1-\Omega^2)^2}}\sin(\Omega\tau+\theta) = \hat{V}\sin(\Omega\tau+\theta) \tag{22}$$

and its derivative with respect to $\Omega\tau$ leads to

$$\phi' = \frac{\alpha\Omega^3}{\sqrt{4\beta^2\Omega^2+(1-\Omega^2)^2}}\cos(\Omega\tau+\theta) = \hat{V}\cos(\Omega\tau+\theta) \tag{23}$$

where

$$\hat{V} = \frac{\alpha\Omega^3}{\sqrt{4\beta^2\Omega^2+(1-\Omega^2)^2}} \quad \text{and} \quad \theta = \arctan(2\beta\Omega, \Omega^2-1). \tag{24}$$

At steady state, ϕ is only a function of $\Omega\tau$, hence the expression of the effective friction function, Eq. (6), simplifies to

$$\bar{\mu}(v_b) = \mu_s\left\langle \operatorname{sgn}(-v_b+\phi'+\Omega^{-1}\dot{\phi})\right\rangle = \mu_s\left\langle \operatorname{sgn}(-v_b+\phi')\right\rangle, \tag{25}$$

where $\dot{z}$ is omitted as it has no contribution in steady-state motion. By inserting Eq. (23) into Eq. (25), the equation of the effective friction function for harmonic excitation with arbitrary frequency becomes

$$\bar{\mu}(v_b) = \mu_s \left\langle \text{sgn}(-v_b + \hat{V}\cos(\Omega\tau + \theta)) \right\rangle = \begin{cases} \mu_s \left(1 - \frac{2}{\pi} \arccos\left(\frac{v_b}{\hat{V}}\right)\right) & \text{for } |v_b| \le \hat{V} \\ \mu_s \text{sgn}(v_b) & \text{for } |v_b| \ge \hat{V}. \end{cases} \tag{26}$$

Eq. (26), combined with Eq. (24), highlights that for large values of Ω, the parameter $\hat{V}$ approaches asymptotically the value of $\alpha\Omega$, which is the amplitude of the harmonically varying term in Eq. (13). Concurrently, the phase angle θ in Eq. (24) tends to vanish. To clarify this observation, Fig. 5(a) compares the relation between the parameter $\hat{V}$ as a function of Ω, with the linear and monotonic trend defined by the amplitude $\alpha\Omega$ of the harmonic varying term in Eq. (13). Fig. 5(b) displays the behavior of θ for increasing values of Ω. The values to generate the plot are reported in the caption of Fig. 5. From Fig. 5, it can be concluded that if Ω lies in the high-frequency regime, the solution of ϕ' provided in Eq. (23), matches the solution shown for ϕ' given in Eq. (11). The comparison highlighted in Fig. 5a also allows to identify a non-dimensional threshold frequency of excitation that discriminates between a high-frequency and near-resonant or low-frequency region. The value of $\Omega_e = 5\omega_n$ could be considered as a possible minimum value of excitation frequency for the high-frequency band. The relative error between $\hat{V}$ and $\alpha\Omega$ at such threshold is 3.9%. It is worth mentioning that the MDSM technique is commonly used for systems subject to high-frequency excitation. However, in the literature, an explicit and proven statement on what the minimum frequency starting from which a high-frequency regime can be defined has never been provided.

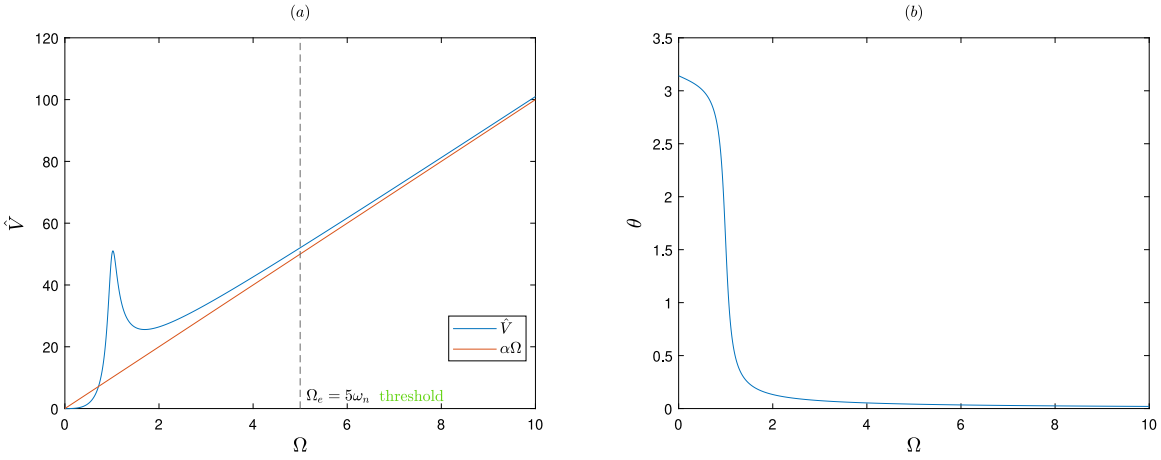

Fig. 5. (a) Coefficient $\hat{V}$ versus Ω; (b) θ versus Ω. Plots obtained for $\beta = 0.1$ and $\alpha = 10$.

While the trend of $\hat{V}$ over the high-frequency regime resembles a linear one, a nonlinear trend is observed near resonance. A rapid increase and decrease can be noticed as soon $\hat{V}$ approaches and exceeds, respectively, the resonance frequency $\Omega_e = \omega_n = 1$. Fig. 6(a) examines closely the latter regime, and specifically four colored markers were placed to inspect the behavior of the corresponding effective friction expression. Fig. 6(b) shows the trend of $\bar{\mu}(v_b)$ with reference to the colored markers in Fig. 6(a). Similarly to what was discussed with reference to Fig. 2, the value of $v_{b,c}$ corresponds to the value of $\hat{V}$ which marks the point after which the effective friction coefficient becomes μ_s and remains constant. As the magnitude of Ω increases from 0, the value of $v_{b,c}$ (=$\hat{V}$) that separates the constant region from the varying one of $\bar{\mu}(v_b)$, increases as well, until the resonance condition is reached (see the red marker and the red line in Figs. 6(a),(b) respectively). For $\Omega \approx 1$ (small damping present), the threshold value of $v_{b,c}$ is $|v_{b,c}| \approx 50$, and it decreases for the further selected points at $\Omega = 1.2$ and $\Omega = 4$ (orange and purple markers and lines, correspondingly). For the high-frequency range, the value of $v_{b,c}$ (or $\hat{V}$) only increases with an increase in Ω.

In Section 2.1, it was mentioned that in the case of the Amontons–Coulomb's law and during a full-slip regime (absence of stick–slip), the solution of the equation of motion for z has no contribution in the steady-state velocity response. Thus, the velocity response can be found by solving the equation of motion for ϕ. This kind of correspondence has never been explicitly pointed out in any previous study with reference to the MDSM technique. It is shown here that such correspondence holds also for the case of the extended version of the MDSM, valid for a general excitation with arbitrary frequency. For the considered system, Eq. (1), the steady-state solution x_{ss} (for $\dot{x} > v_b$) is

$$x_{ss} = \frac{\alpha\Omega^2}{\sqrt{4\beta^2\Omega^2 + (1-\Omega^2)^2}} \sin(\Omega\tau + \theta) + \mu_s \tag{27}$$

and its derivative then becomes

$$\dot{x}_{ss} = \frac{\alpha\Omega^3}{\sqrt{4\beta^2\Omega^2 + (1-\Omega^2)^2}} \cos(\Omega\tau + \theta) = \hat{V}\cos(\Omega\tau + \theta) = \phi' \tag{28}$$

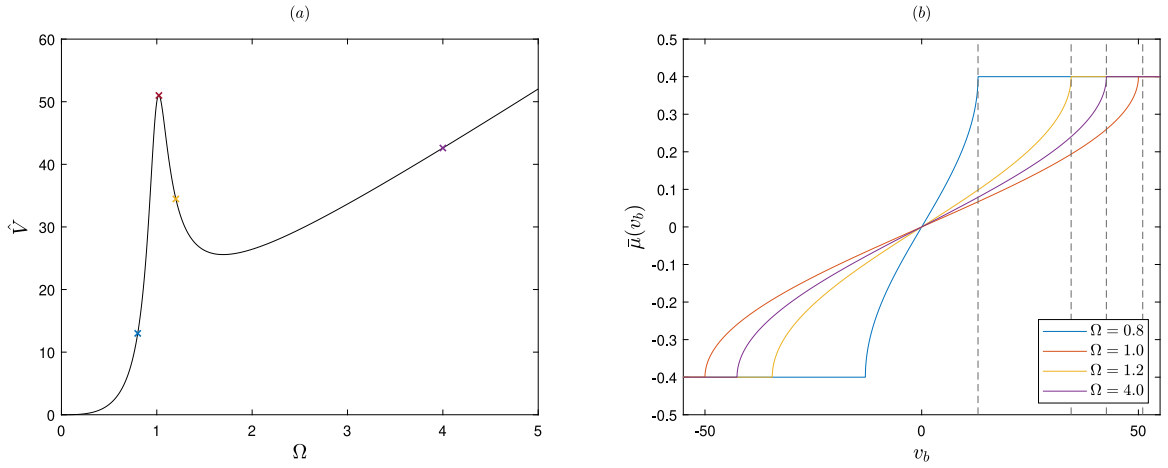

Fig. 6. (a) $\hat{V}$ versus Ω; (b) $\bar{\mu}(v_b)$ behavior for different excitation magnitudes. Plots obtained for $\beta = 0.1$ and $\alpha = 10$. The colored markers in (a) are linked to the corresponding colored lines in (b).

The expression of $\dot{x}_{ss}$ would be the same for $\dot{x} < v_b$ as well, as the contribution of the friction force within the particular solution given in Eq. (27) is provided by a constant ($\pm\mu_s$). Therefore, Eq. (28) exactly corresponds to the derivative of motion ϕ' given in Eq. (23). The expression $\hat{V}$ corresponds to the amplitude of the velocity response function of the system (Eq. (1)), subject to the Amontons–Coulomb's friction force and considering a sliding regime (absence of stick–slip motion). The correspondence between $\hat{V}$ and the system's velocity response function facilitates the interpretation of the vibration-induced effects on the friction force, hence, avoiding cumbersome calculations to find the expression of ϕ' for an arbitrary frequency using the extended MDSM. The effective friction force function $\bar{\mu}(v_b)$ and the expression for ϕ' can be straightforwardly found by means of the velocity response function of the given system. Comparing the cases presented in Sections 2.1–2.2 (MDSM and the model used in [16,17]), the effective friction force expression seemed to come out mainly from mathematical considerations, while, as revealed here, it is actually part of a physical process related to the velocity response of the system. While for high frequency the effective friction expression is driven by the velocity solely induced by inertial effects, as the frequency of excitation decreases, the influence of damping and stiffness forces come into play.

Lastly, to validate the analytical results numerically, a comparison of the analytical solution of $\bar{\mu}(v_b)$ (solid line) versus the numerical solution of $\bar{\mu}(v_b)$ (dashed line), for the case of a low-frequency and high-frequency excitation (high and low relative to the natural frequency of the system) is shown in Fig. 7(a) and (b), respectively. Note that the numerical solution (steady state)

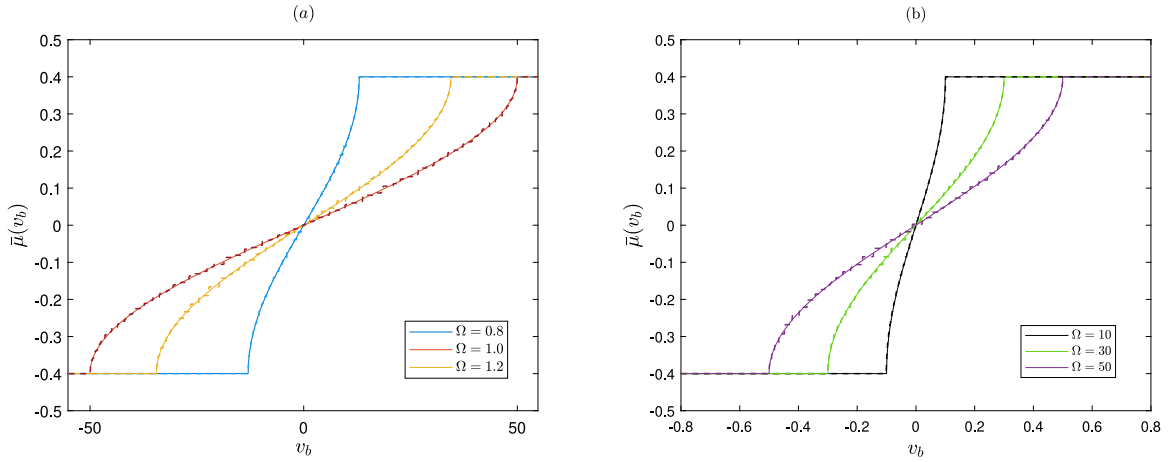

Fig. 7. (a) Comparison of numerical (dashed line) and analytical (solid line) solutions of effective friction for the case of low-frequency excitation; (b) Same comparison for the case of high-frequency excitation ($\beta = 0.1$ and $\alpha = 10$).

of ϕ', Eq. (19), is obtained for a set of parameter values in which no stick–slip occurs. In both figures, it can be observed that the analytical solution matches the numerical one, proving that the analytical solutions of ϕ' and $\bar{\mu}(v_b)$ are correct. The following section will demonstrate that the velocity response function can not only be exploited to calculate the effective friction expression but also to define the boundaries of the transition between the stick and slip regimes.

3. Implications to stick–slip analysis for an oscillator and belt system

As highlighted in this study, the expression of the effective friction force for a generic harmonic excitation is obtained for the steady-state oscillatory motion in continuous sliding. However, for certain belt velocities, excitation amplitudes and frequencies, stick–slip might occur, making the analytical expressions, such as Eq. (26), invalid. Thus, it is crucial to define the boundaries of the transition from the stick–slip to the slip regime. To achieve this, the analysis performed by den Hartog [40] in his seminal work is first considered. The investigated model is a single mass–spring–damper system with Amontons–Coulomb's law, similar to the one presented in Fig. 1, but without the moving belt. For this system, the stick–slip boundaries are defined by the graph shown in Fig. 8(a), as a function of the ratio between forcing and natural frequency $\Omega = \Omega_e/\omega_n$ and the ratio between friction force and excitation amplitude $\mu_s N/mr\Omega_e^2$ for different values of damping ratio β. The region below the lines defines the continuous-slip regime and the one above indicates the stick–slip regime.

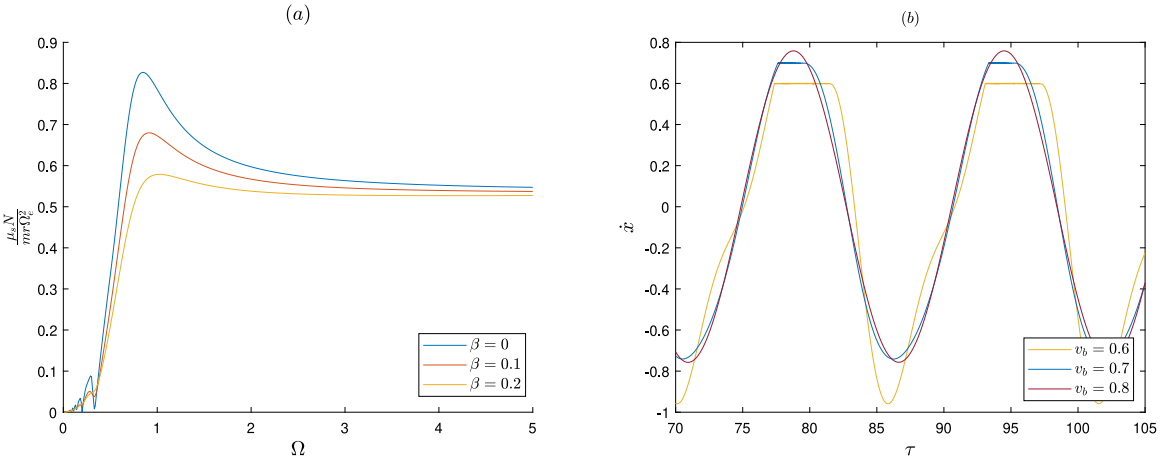

Fig. 8. (a) Stick–slip boundary for a damped SDOF system subjected to harmonic excitation (see [40]); (b)Velocity response for different belt velocities, $\beta = 0.1$, $\alpha = 10$, and $\Omega = 0.4$.

Using the graph for specific values of μ_s, β and excitation amplitude, the range of frequencies for which the mass is in continuous-slip motion can be determined. For these frequencies, regardless of the presence of the moving belt and the corresponding belt velocity, the mass will always be characterized by a continuous-slip motion, provided no dependency between friction force and slip velocity magnitude is assumed. The presence of a moving belt only shifts the equilibrium position around which the mass oscillates. For the range of frequencies for which stick–slip is present in den Hartog's model, the presence of the belt and its corresponding velocity plays an important role in eliminating stick–slip. For the latter case, the condition presented below is necessary

$$V_b > |\hat{V}|. \tag{29}$$

If the belt velocity is larger than $|\hat{V}|$, the relative velocity between the mass and the belt will not cross zero, hence stick–slip will not occur. This finding was already discussed in [35], and it is important to highlight here that $|\hat{V}|$ simply corresponds to the amplitude of the velocity response function. Therefore, if for a certain excitation frequency stick–slip is present for $V_b = 0$, to eliminate stick–slip, V_b should simply be bigger than the magnitude of the velocity response function (obtained assuming continuous slip) for that excitation frequency.

As an example, Fig. 8(b) shows the velocity responses of a SDOF system for different V_b values. The tangential excitation frequency is the same for all cases and, when assuming continuous slip, the corresponding amplitude of $\hat{V} = 0.76$ is identified. Fig. 8(b) shows that for $V_b < \hat{V}$ stick–slip is present while for $V_b > \hat{V}$, the motion is continuous. Thus, to prevent stick–slip, a belt velocity $V_b > \hat{V}$ is necessary. With reference to the effective friction expression, see Eq. (26) and Fig. 6(b), and for the specific case of assuming the Amontons–Coulomb's law, the condition of $V_b > \hat{V}$ results in no variation of the friction force. Thus, before performing an analysis to calculate the effective friction for a specific excitation frequency, the first step is to check whether stick–slip or continuous-slip motion is present for the case with a non-moving belt (den Hartog's model). If the latter system is in continuous-slip motion, the effective friction of the actual system can be calculated for any belt velocity. If den Hartog's model is in stick–slip regime for a specific excitation frequency, a belt velocity higher than the amplitude of the velocity response function (obtained assuming continuous slip) will eliminate stick–slip. In the case of Amontons–Coulomb's law (no dependence between friction force and magnitude of slip velocity) this also leads to no variation of the friction force due to the high belt velocity. While the illustrative example presented here only refers to a single-degree-of-freedom system, as it will be shown in the next section, the same conclusion holds for a multi-degree-of-freedom system as well.

4. Vibration-induced friction modulation for a harmonically forced 2-DOF system in sliding regime

The following section makes use of the extended MDSM to quantify the vibration-induced effect on friction for a multi-degree-of-freedom system in the absence of any stick regime. Different load directions and combinations are considered. The results are then compared to each other and to the ones obtained by exploiting the velocity response function of the system, which allows bypassing the cumbersome mathematical steps needed for the extended MDSM.

4.1. Description of the harmonically forced 2-DOF system

To illustrate the procedure, a two-degree-of-freedom (2-DOF) model is investigated as shown in Fig. 9. The system consists of a mass M positioned on a belt moving at a constant speed V_b. The mass is being held in position by two linear springs with stiffnesses K_1 and K_2, and by two linear dashpots with damping coefficients C_1 and C_2, for which subscript 1 and 2 refer to the parallel and normal direction with respect to the belt surface, respectively. The spring K_2 and the dashpot C_2 are respectively considered as the normal contact stiffness and damping between the objects in relative sliding motion. Regarding the external load, three cases will be studied: tangential loading only, normal loading only, and the combination of these two, as shown in Fig. 9. For all the considered loading scenarios, the external harmonic loading is characterized by a frequency Ω_e and amplitude $M\alpha\Omega_e^2$.

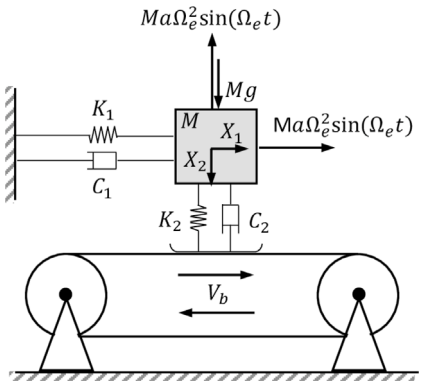

Fig. 9. Layout of the 2-DOF system subject to external harmonic loads in the normal and tangential directions.

If no external loading is present, the equations of motion for the 2-DOF system read as follows

$$M\ddot{X}_1 + C_1\dot{X}_1 + K_1X_1 + F_f = 0 \tag{30}$$

$$M\ddot{X}_2 + C_2\dot{X}_2 + K_2X_2 - Mg = 0 \tag{31}$$

where F_f is the frictional force. As mentioned earlier, the frictional force F_f is assumed to obey Amontons–Coulomb's law, given by $F_f = \mu(V_r)F_n$ with $\mu(V_r)$ referring to the dimensional form of Eq. (3). In this study, we assume the normal force, F_n, to be dependent on the contact stiffness and the damping in the X_2 direction. Therefore, the expression of the friction force becomes

$$F_f = \mu(V_r)F_n = \mu(V_r)(C_2\dot{X}_2 + K_2X_2). \tag{32}$$

This expression for F_f is chosen to demonstrate the effect of the contact resonance on the effective friction expression. The equations of motion of the system in the absence of an external load can be rewritten in a more generic form as

$$\begin{bmatrix}1 & 0\\ 0 & 1\end{bmatrix}\begin{pmatrix}\ddot{X}_1\\ \ddot{X}_2\end{pmatrix} + \begin{bmatrix}2\beta_1\omega_1 & 0\\ 0 & 2\beta_2\omega_2\end{bmatrix}\begin{pmatrix}\dot{X}_1\\ \dot{X}_2\end{pmatrix} + \begin{bmatrix}\omega_1^2 & 0\\ 0 & \omega_2^2\end{bmatrix}\begin{pmatrix}X_1\\ X_2\end{pmatrix} + \begin{pmatrix}\mu(V_r)(2\beta_2\omega_2\dot{X}_2 + \omega_2^2X_2)\\ -g\end{pmatrix} = \begin{pmatrix}0\\ 0\end{pmatrix} \tag{33}$$

where $\beta_i = \frac{C_i}{2M\omega_i}$ and $\omega_i^2 = \frac{K_i}{M}$ and $i = 1, 2$. In the following subsection, the first loading case, that of tangential load only will be investigated.

4.2. Tangential harmonic loading

If only a tangential harmonic load is considered, the right hand side of Eq. (33) containing the external loading $\mathbf{F}_{ext}$ becomes

$$\mathbf{F}_{ext} = \begin{pmatrix}\alpha\Omega_e^2\sin(\Omega_e t)\\ 0\end{pmatrix}. \tag{34}$$

As mentioned in Section 3, the first step is to define the stick–slip boundary. According to [40], the boundary is defined by the graph shown in Fig. 8(a), as a function of the ratio between forcing and natural frequency $\Omega = \Omega_e/\omega_1$ and the ratio between friction force and excitation amplitude (the latter being $\mu_s N/mr\Omega_e^2$ for the SDOF) for different values of damping ratio β. In this case, since no

external load is present in the X_2 direction, no motion will occur in this direction. The system then reduces to a SDOF one and the ratio between friction force and excitation amplitude becomes $\mu_s g/\alpha\Omega_e^2$. Fig. 10 shows the graph defining the stick–slip boundary and the graph of $\mu_s g/P_t$, where $P_t = \alpha\Omega_e^2$ is the amplitude of the tangential external force in Eq. (34). As shown in Fig. 10, for frequencies $\Omega = \Omega_e/\omega_1$ higher than approximately 0.78, the mass will be in the sliding regime. For these frequencies, analytical expressions for the effective friction are valid.

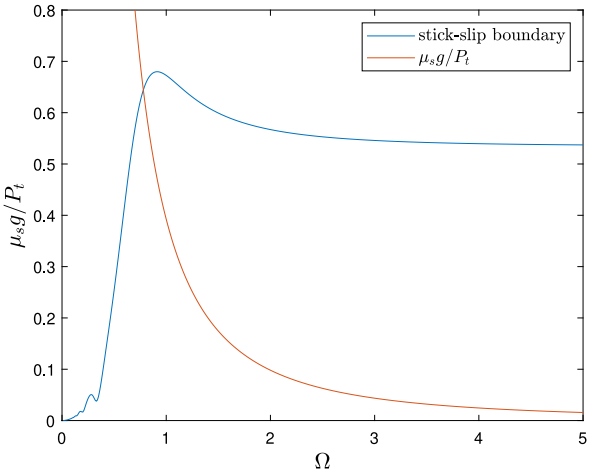

Fig. 10. Stick–slip boundary for the 2-DOF system with external loading applied in tangential direction only ($\alpha = 10$ and $\mu_s = 0.4$).

Having defined the stick–slip boundary, the effective friction expression $\bar{\mu}(V_b)$ can be derived using the extended MDSM. However, since the loading is applied in the tangential direction only and the system reduces to a single-degree-of-freedom one, the effective friction characteristic is the same as in Section 2.2 (valid for Ω higher than approximately 0.78). This correspondence holds since the value of $\omega_1 = 1$ and the used values of β_1 and α are the same for both cases. In the next subsection, the 2-DOF system subject to a normal harmonic loading only (index n referring to the latter) is considered.

4.3. Normal harmonic loading

When the system represented in Fig. 9 is only subject to the normal loading, the right-hand side of Eq. (33) containing the external loading $\mathbf{F}_{ext}$ becomes

$$\mathbf{F}_{ext} = \begin{pmatrix} 0 \\ -\alpha\Omega_e^2 \sin(\Omega_e t) \end{pmatrix}. \tag{35}$$

Since motion is present in the X_2 direction and since the tangential friction force F_f, Eq. (32), depends on X_2 and $\dot{X}_2$, mode coupling is present due to the friction force and motion is expected to be exhibited in both directions. To ensure an analytical solution for full vibration cycles, it should be noted that the amplitude of oscillation in the X_2 direction should be smaller than the static contact compression given by

$$X_{2,0} = \frac{Mg}{K_2} = \frac{g}{\omega_2^2}, \tag{36}$$

in which case the mass is always in contact with the belt. For amplitudes of vertical oscillation higher than $X_{2,0}$, the belt is in a state of intermittent contact (jumping case). Fig. 11 shows a comparison of the limit $X_{2,0}$ with the amplitude of displacement in the X_2 direction for a range of α and Ω_e. As the displacement values are below the limit, for the parameters considered in the study, the mass is always in contact with the belt. It should be noted that different parameters such as a higher amplitudes of excitation or lower damping will result in higher amplitudes of displacement in the X_2 direction, and eventually in jumping scenarios for which the analytical results on friction modulation are not valid.

To ensure that stick–slip is not occurring, the same analysis as described in Section 3 for the SDOF should be performed now considering the 2-DOF system. As mentioned in Section 3, the first step is to check whether slick-slip or continuous sliding is present for the case with a non-moving belt (den Hartog's model). For the 2-DOF system with normal load only, and with friction force described as in Eq. (32), if a non-moving belt is present, no motion is occurring in the tangential direction. For oscillations to be present in this direction, a moving belt is necessary. Then, a belt velocity higher than the amplitude of the velocity response function (obtained assuming continuous slip) will ensure continuous sliding. Since Amontons–Coulomb's law is assumed (no dependence between friction force and the magnitude of slip velocity), this also leads to no variation of the friction force due to the high belt velocity. Thus, for the 2-DOF system with normal loading only, the mass will be in continuous sliding only for belt velocities higher than the amplitude of the velocity response function (obtained assuming continuous slip), for which no friction change will be observed. Since this loading case leads to no friction change, there is no need to neither solve for the equations of motion for $\mathbf{\Phi}$ (see

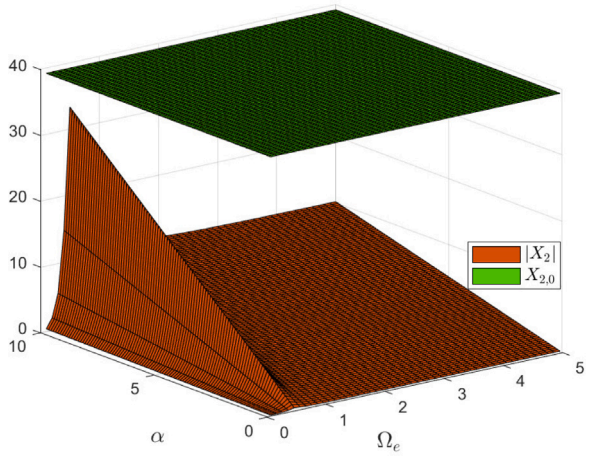

Fig. 11. Comparison of the amplitude of displacement $|X_2|$ (orange), and the static contact compression $X_{2,0}$ (green) for a range of α and Ω_e ($\omega_1 = 1$, $\omega_2 = 0.5$, $\beta_1 = 0.1$, $\beta_2 = 0.15$, $\alpha = 10$ and $\mu_s = 0.4$). (For interpretation of the references to color in this figure legend, the reader is referred to the web version of this article.)

Appendix A.1) nor to compute the velocity response function. In the next subsection, these analyses are performed for a general setup subjected to harmonic loads in different directions.

4.4. General harmonic load setup

When both tangential and normal loading is present, the right-hand side of Eq. (33) containing the external loading $\mathbf{F}_{ext}$ becomes

$$\mathbf{F}_{ext} = \begin{pmatrix} \alpha\Omega_e^2 \sin(\Omega_e t) \\ -\alpha\Omega_e^2 \sin(\Omega_e t) \end{pmatrix}. \tag{37}$$

which is a superposition of the tangential force, Eq. (34), and the normal force, Eq. (35). Since the normal loading is the same as in Section 4.3, the mass is in continuous contact (provided the parameter values chosen are the same). The next step is to define the stick–slip boundary, for which the ratio between the friction force and the excitation amplitude for the motion in the X_1 direction should be calculated. Considering a non-moving belt and $\dot{X}_1 < 0$ (as in [40]), the equation of motion is

$$\ddot{X}_1 + 2\beta_1\omega_1\dot{X}_1 + \omega_1^2 X_1 - \mu_s(2\beta_2\omega_2\dot{X}_2 + \omega_2^2 X_2) = \alpha\Omega_e^2 \sin(\Omega_e t). \tag{38}$$

The expressions for X_2 and $\dot{X}_2$ can be found by solving the equation of motion in the vertical direction. Eq. (38) then becomes

$$\ddot{X}_1 + 2\beta_1\omega_1\dot{X}_1 + \omega_1^2 X_1 - \mu_s g = -\frac{\mu_s\alpha\Omega_e^2(\omega_2^2 \sin(\Omega_e t + \theta) + 2\beta_2\omega_2\Omega_e \cos(\Omega_e t + \theta))}{\sqrt{4\beta_2^2\omega_2^2\Omega_e^2 + (\omega_2^2 - \Omega_e^2)^2}} + \alpha\Omega_e^2 \sin(\Omega_e t) \tag{39}$$

and the excitation amplitude is found using the terms on the right-hand side. Note that the static contribution of the contact force, i.e. the $\mu_s g$ term is written on the left-hand side of the equation. Fig. 12(a) shows the graph defining the stick–slip boundary and the graph of $\mu_s g / P_{tn}$, where P_{tn} is the amplitude of the harmonic force in the right-hand side in Eq. (39). As it is shown in the figure, for frequencies $\Omega = \Omega_e/\omega_1$ higher than ≈0.84 the mass will be in the sliding regime. For these frequencies, the analytical expressions for the effective friction will be valid.

To obtain the effective friction expression, first the extended MDSM is used and the equations of motion for $\mathbf{\Phi}$ are solved analytically as shown in Appendix A.1. All expressions of the coefficients of the harmonics (i.e., $B_{11}(\tau)$, $B_{12}(\tau)$, $B_{21}(\tau)$ and $B_{22}(\tau)$) approach to a constant value as τ increases reaching a steady-state condition (see Appendix A.1) and the expression for Φ_1' in steady state is

$$\Phi_1' = \hat{V}_{tn} \cos(\Omega_e \tau + \theta_{tn}), \tag{40}$$

where

$$\hat{V}_{tn} = \frac{\alpha\Omega_e^3\sqrt{4\beta_2^2\omega_2^2\Omega_e^2(\mu_s + 1)^2 + (\omega_2^2 - \Omega_e^2)^2 + \mu_s\omega_2^2(\mu_s\omega_2^2 - 2\Omega_e^2 + 2\omega_2^2)}}{\sqrt{(4\beta_1^2\omega_1^2\Omega_e^2 + (\omega_1^2 - \Omega_e^2)^2)(4\beta_2^2\omega_2^2\Omega_e^2 + (\omega_2^2 - \Omega_e^2)^2)}}. \tag{41}$$

for which index tn refers to tangential-normal loading. Since coupling between the two degrees of freedom is present due to the assumed friction law, differently from the tangential loading case, there is a dependence between $\hat{V}_{tn}$ and μ_s. Moreover, since

oscillations are occurring in both directions, $\hat{V}_{tn}$ depends also on the system characteristics (mass, stiffness and damping values) in both directions and on the amplitude and frequency of excitation.

Next, the velocity response function $\hat{Y}_1(\Omega_e)$ is found using Eqs. (A.6)–(A.10), Appendix A.2, with $\mathbf{F}_{ext}$ represented as in Eq. (37). In Fig. 12(b), a comparison of $|\hat{Y}_1(\Omega_e)|$ with $\hat{V}_{tn}$ for a range of μ_s values is shown. The plot of $|\hat{Y}_1(\Omega_e)|$ coincides with that of $\hat{V}_{tn}$, and both of them approach the trend of the velocity amplitude given by the high-frequency excitation only as the frequency increases. The stick–slip regime is also indicated in the figure in magenta. An increase in μ_s value results in an increase in the stick–slip regime. While oscillations occur in both directions, the first peak is very small due to the used damping and excitation amplitude values. For lower damping values, or higher oscillation amplitudes, the first peak would be more visible, however the mass might be in intermittent contact.

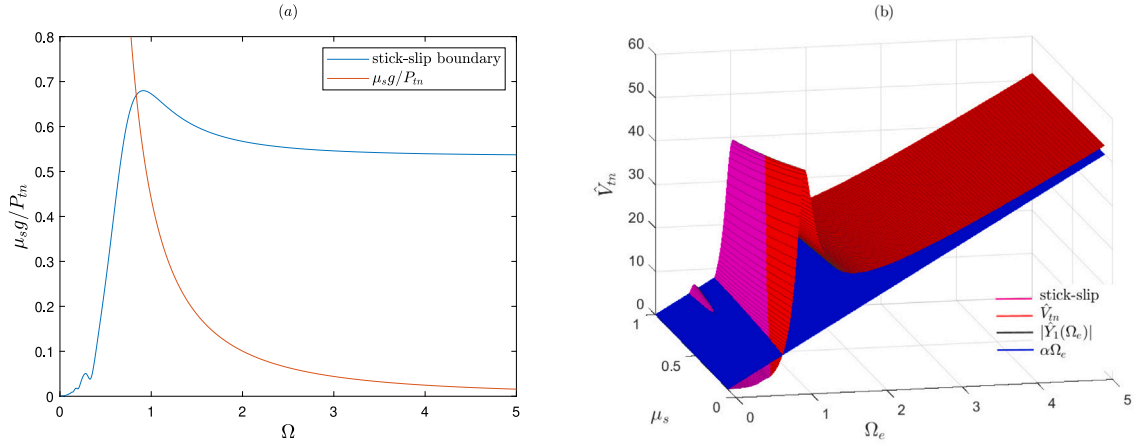

Fig. 12. (a) Stick–slip boundary for the 2DOF system with external loading applied in tangential and normal directions ($\mu_s = 0.4$); (b) Comparison of $|\hat{Y}_1(\Omega_e)|$ (black lines), $\hat{V}_{tn}$ (red surface) and amplitude of the Φ_1' for high-frequency excitation (blue plane) for a range of μ_s values. Parameters as in Fig. 11. The magenta color defines the parameter space for which stick–slip occurs. (For interpretation of the references to color in this figure legend, the reader is referred to the web version of this article.)

If the phase of the harmonic tangential load changes by 180° (a switch from an initial positive $+X_1$ to an initial negative direction $-X_1$ with respect to the considered reference system), the stick–slip boundary, the velocity response function, and eventually the effective friction, change as well. Fig. 13(a) shows the graph defining the stick–slip boundary for this case. As it is shown in the figure, for frequencies $\Omega = \Omega_e/\omega_1$ higher than ≈0.72, the mass will be in the sliding regime and the analytical solutions for the effective friction force expression will be valid. Compared to Fig. 12(a), the sliding regime occurs in a slightly larger parameter space, meaning that the initial loading phase has an influence on the stick–slip regime as well. In Fig. 13(b), the plots of $|\hat{Y}_1(\Omega_e)|$ and $\hat{V}_{tn}$ for an initial negative tangential loading are illustrated. The stick–slip boundary is displayed as well. Again, the graph of $|\hat{Y}_1(\Omega_e)|$ coincides with that of $\hat{V}_{tn}$, and both of them approach the trend of the velocity amplitude given by the high-frequency excitation only as the frequency increases.

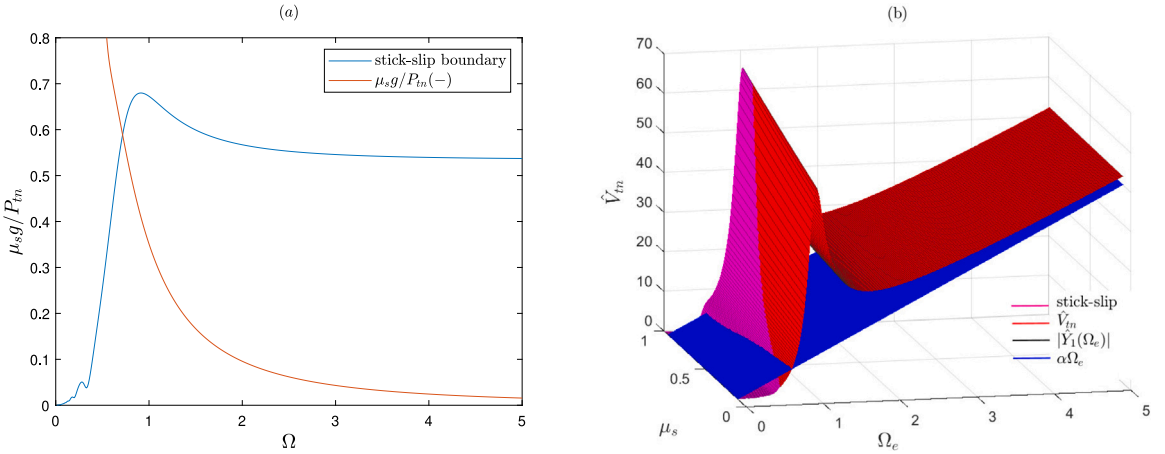

Fig. 13. (a) Stick–slip boundary for the 2-DOF system with external loading applied in tangential and normal directions. Tangential loading initially applied in the $-X_1$ direction ($\mu_s = 0.4$); (b) Comparison of $|\hat{Y}_1(\Omega_e)|$ (black lines), $\hat{V}_{tn}$ (red surface) and amplitude of the Φ_1' for high-frequency excitation (blue plane) for a range of μ_s values. Tangential loading initially applied in the $-X_1$ direction. Parameters as in Fig. 11. The magenta color defines the parameter space for which stick–slip occurs. (For interpretation of the references to color in this figure legend, the reader is referred to the web version of this article.)

A comparison of the amplitudes of the velocity response functions for the three loading cases (tangential, general with initial tangential loading in $+X_1$, and general with initial tangential loading in $-X_1$) for $\mu_s = 0.4$ is presented in Fig. 14(a). From the figure, it can be observed that as the excitation frequency increases, the amplitudes of the velocity response function coincide. Thus, for high frequencies, the results of the effective friction expression are the same independent of the loading configuration. While the plot in Fig. 14(a) is obtained for one value of μ_s, from the 3D plots shown in Fig. 12(b) and in Fig. 13(b), it can be observed that this conclusion holds for any μ_s value. Looking at low frequencies, however, the plots obtained for each loading case do not coincide, meaning that nearby resonance, the effective friction expression depends on the type of loading applied. Fig. 14(b) shows the comparison of the effective friction expression for these three loading cases and $\Omega_e = 1$. For this value of the excitation frequency, from Fig. 14(a), it can be observed that the normal-tangential loading case $(-X_1)$ will result in a higher amplitude of the velocity response function, followed by the tangential loading case and lastly by the normal-tangential loading $(+X_1)$. This trend is confirmed by the effective friction plots portrayed in Fig. 14(b). The loading case with higher amplitude in the velocity response is characterized by a slightly larger parameter space of V_b for which a friction force decrease can be observed.

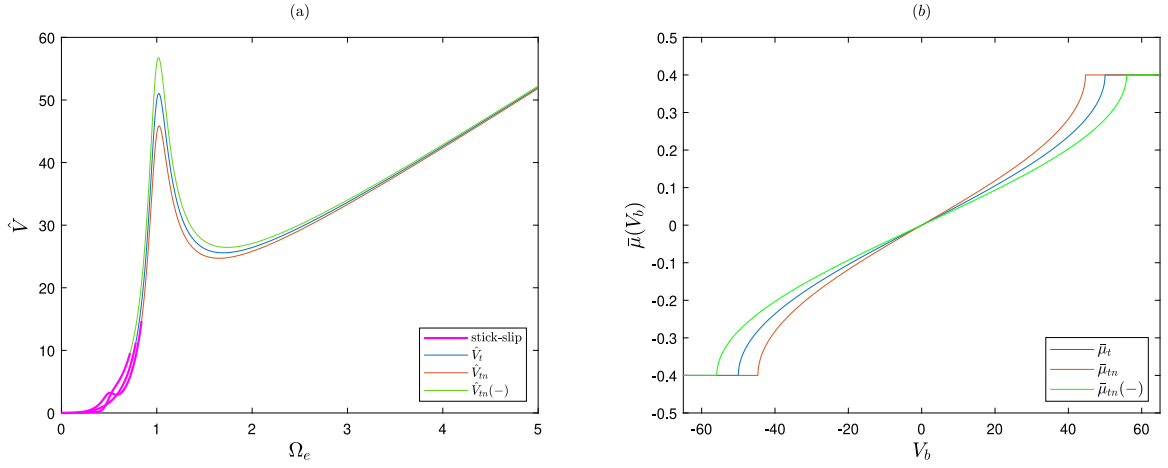

Fig. 14. (a) Comparison of $\hat{V}$ for all 3 loading cases, tangential (blue), normal-tangential $(+X_1)$ (orange), normal-tangential $(-X_1)$ (green), for $\mu_s = 0.4$; (b) Comparison of $\bar{\mu}(V_b)$ for the same loading cases and $\Omega_e = 1$. Parameters as in Fig. 11. The magenta line defines the parameter space for which stick–slip occurs. (For interpretation of the references to color in this figure legend, the reader is referred to the web version of this article.)

For the parameter values used so far, from Figs. 12(a) and 13(a), it can be seen that for excitation frequencies near the contact resonance, the mass is stick–slipping. If other parameter values are considered, however, it would be possible to obtain an effective friction graph near contact resonance as well. For example, for $\mu_s = 0.1$, $\omega_2 = 2$, $\alpha = 1$, and a vertical preload of $P = Mg$ acting on the mass in X_2 direction, at contact resonance, the 2 DOF system will be in continuous sliding contact. As the ω_2 value has increased, the amplitude of the displacement response in X_2 direction increases as well. That is why a preload and lower α values are necessary to prevent an intermittent contact. However, lower values of α lead to stick–slip in the horizontal direction. To prevent the latter, a lower μ_s value is used. For this parameter space, the stick–slip boundary shows that excitation frequencies $\Omega_e > 1.15$ results in sliding. Fig. 15 shows the velocity response function of the 2-DOF system subjected to both normal and tangential load (in $+X_1$ direction) for $\omega_2 = 2$, $\alpha = 1$ and for $\mu_s = 0.1$ (left) and a range of μ_s (right). The rest of the parameters remain the same as in Fig. 11. The stick–slip regime is also shown in magenta indicating that higher μ_s values result in stick–slip. Moreover, since different ω_2 and α values are used, both peaks are clearly visible in the figure.

A comparison between the amplitudes of the velocity response functions for the three loading cases (tangential, general with initial tangential loading in $+X_1$, and general with initial tangential loading in $-X_1$) for $\mu_s = 0.1$ is presented in Fig. 16(a). The stick–slip parameter space is always defined by the magenta line. It can be seen that, as the excitation frequency increases, the amplitudes of each case approach each other, showing the same trend as in Fig. 14(a). However, moving towards the resonance peaks, the behavior changes. Fig. 16(b) shows the effective friction plots for each loading case and $\Omega_e = \omega_2 = 2$, so that a continuous sliding regime is ensured for each load case. For this value of the excitation frequency, from Fig. 16(a), it can be observed that the normal-tangential loading case $(+X_1)$ will result in a higher amplitude of the velocity response function, followed by the tangential loading only and lastly by the normal-tangential loading $(-X_1)$ case. This trend is confirmed by the effective friction plots portrayed in Fig. 16(b). Note that the effective friction changes if a different excitation frequency is considered. The effective friction trend is also different from that in Fig. 14(b). While in Fig. 14(b), the normal-tangential loading $(-X_1)$ results in the highest friction decrease (comparing for $\Omega_e = 2$), in Fig. 16(b) the normal-tangential loading $(+X_1)$ gives the largest friction change. Thus, a different dynamic characteristic of the system and different forcing parameter result not only in different stick–slip/sliding regimes but also in different effective friction values. Furthermore, upon examining Fig. 16(a), it is evident that the $\hat{V}$ values for the three loading scenarios exhibit the greatest discrepancy at $\Omega_e \approx 1.8$, which is in proximity to the contact resonance frequency. This suggests that the dissimilarity in effective friction values between each load case would be most notable at this specific frequency. Hence, it

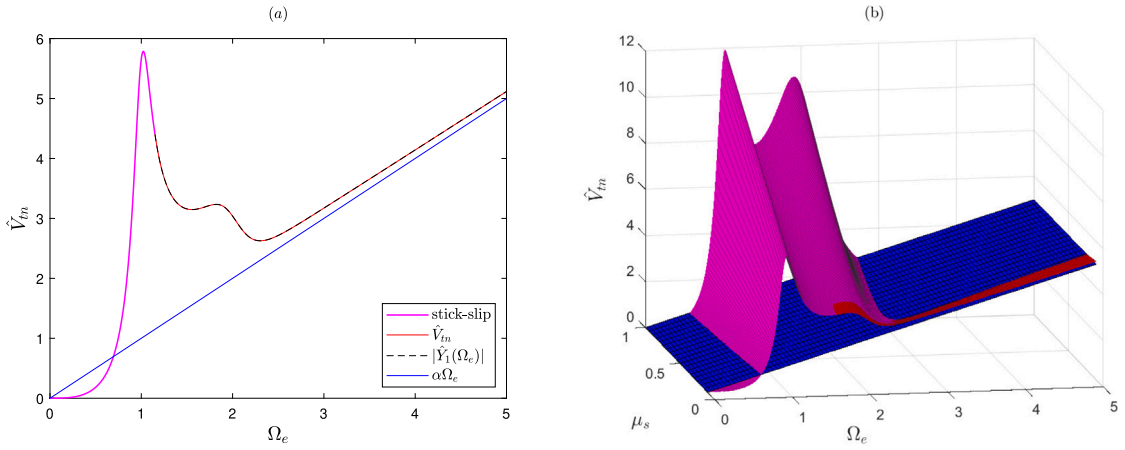

Fig. 15. (a) Comparison of $|\hat{Y}_1(\Omega_e)|$ (black dashed line), $\hat{V}_{tn}$ (red continuous line) and amplitude of the Φ_1' for high-frequency excitation (blue continuous line) for $\mu_s = 0.1$; (b) Comparison for a range of μ_s values. $\omega_2 = 2$, $\alpha = 1$ and the rest of parameters as in Fig. 11. The magenta color defines the parameter space for which stick–slip occurs. (For interpretation of the references to color in this figure legend, the reader is referred to the web version of this article.)

can be concluded that incorporating a friction force that somehow depends on the normal contact stiffness into the model, has a considerable impact on the effective friction values, particularly when the excitation frequencies are near the contact resonance. Besides the modeling implications, the pattern shown in Fig. 16 nearby the contact resonance for different loading cases, can also be used as a characteristic feature during experiments to eventually confirm (or disprove) for a given friction pair, the dependence of the friction force on the normal contact stiffness and damping.

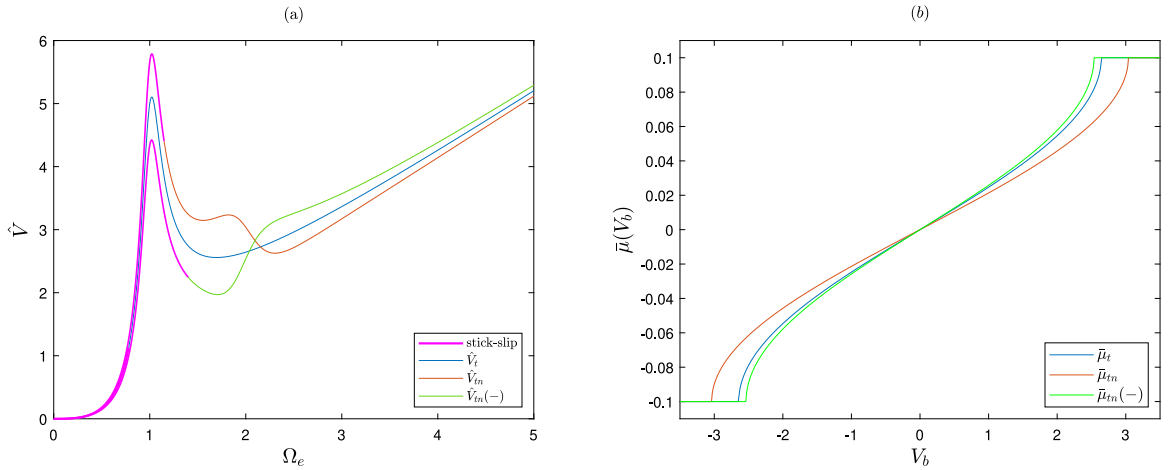

Fig. 16. (a) Comparison of $|\hat{Y}_1(\Omega_e)|$ for all 3 loading cases, tangential (blue), normal-tangential ($+X_1$) (orange), normal-tangential ($-X_1$) (green), for $\mu_s = 0.1$; (b) Comparison of $\bar{\mu}(V_b)$ for the same loading cases and $\Omega_e = 2$. $\omega_2 = 2$, $\alpha = 1$ and the rest of parameters as in Fig. 11. The magenta line defines the parameter space for which stick–slip occurs. (For interpretation of the references to color in this figure legend, the reader is referred to the web version of this article.)

It is worth highlighting that the conclusions drawn so far for the effective friction expression of the 2-DOF system subjected to different load configurations are dependent on the choice of the friction force F_f. The friction force F_f as a function of F_n, Eq. (32), was chosen to demonstrate the effect of the contact resonance. If F_n is assumed to be proportional to the inertial force in the vertical direction, the F_f expression becomes

$$F_f = \mu(V_r) M \ddot{X}_2 = \mu(V_r)(-\alpha\Omega^2 \sin(\Omega\tau) + g), \tag{42}$$

where $M\ddot{X}_2$ is found using the equation of motion in X_2 direction after neglecting the stiffness and damping terms. Considering this friction force expression, the velocity response functions are calculated again. A comparison of their amplitudes for two loading cases and for $\mu_s = 0.4$ is presented in Fig. 17(a) where the continuous-line plots are obtained using F_f as in Eq. (32) and the dashed-line plots using F_f as in Eq. (42). Note that the tangential loading case is not portrayed in the figure because when only tangential loading is present both expression of F_f (Eqs. (32) and (42)) are the same, i.e. $F_f = Mg\mu(V_r)$, as there is no displacement in the X_2 direction.

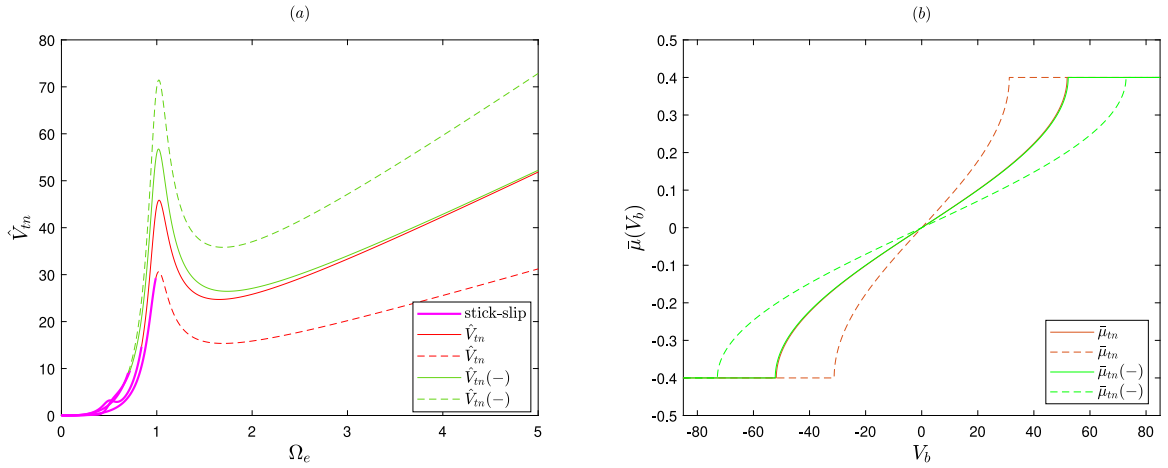

Fig. 17. (a) Comparison of $|\hat{Y}_1(\Omega_e)|$ for 2 loading cases where continuous lines obtained using F_f as in Eq. (32) and dashed line using F_f as in Eq. (42), for $\mu_s = 0.4$; (b) Comparison of $\bar{\mu}(V_b)$ for the same loading cases and $\Omega_e = 5$. Parameters as in Fig. 11. The magenta line defines the parameter space for which stick–slip occurs. (For interpretation of the references to color in this figure legend, the reader is referred to the web version of this article.)

From the figure, it can be observed that when the friction force depends only on the inertial force in the normal direction (dashed lines), as the excitation frequency increases, the amplitudes of the velocity response function do not coincide anymore. This is to be expected because the inertial force prevails at high frequencies. Fig. 17(b) shows the comparison of the effective friction expression for these loading cases and for $\Omega_e = 5$. While the continuous lines coincide, the dashed lines display different effective friction plots, complying to the velocity response function trends portrayed in Fig. 17(a). This enforces the fact that the nature of the contact normal force affects the results of the effective friction expression, especially as we go towards the high-frequency regime. To reconnect to the conclusion drawn for Fig. 16, to assess whether a contact normal force is mainly driven by a compliant force (characterized by a contact resonance and contact damping) or by the inertial contribution in the vertical direction, the measurement of the velocity response functions for different loading cases would enable such discrimination, as shown in Figs. 16(a) and 17(a).

Note that, if the 2-DOF system considered so far included a diagonal spring (oriented at an oblique angle of 45° relative to the normal direction), mode coupling will always be present. Different values of the diagonal spring's stiffness would result in different shapes and trends of the velocity response functions. The latter can then be used to calculate eventual vibration-induced friction modulation. However, in such case, the system could be prone to mode coupling instabilities [31], that should be taken into account before assessing the effective friction characteristic at steady state.

To conclude the analysis done so far, it can be stated that the velocity response function can be used to obtain the effective friction expression for a multi-degree of freedom system and for a general frequency range of excitation. The influence of the external loadings on friction depends on the combination of loading phase, excitation frequency, system characteristics (mass, stiffness and damping values) and the value of the static friction coefficient. Depending on these parameters, applying two loads does not necessarily result in a higher friction change compared to the application of only one type of load. Lastly, the values of effective friction greatly depend on the choice of the friction force expression, inclusive of the normal contact force.

5. Conclusions

In this work, the Method of Direct Separation of Motion (MDSM) was extended to quantify the vibration-induced effect on the average friction force for a single and a multi-degree-of-freedom system, subject to different combinations of dynamic load directions and valid for any frequency of excitation (low- and high-frequency regime). The systems considered are influenced by a friction force represented by the Amontons–Coulomb's law, using different expressions of the normal contact force, representing a compliant and a rigid contact case. The extension enabled to identify a threshold, $\Omega = 5\omega_n$, limiting the so-called "high-frequency" regime for vibration-induced friction modulation. The MDSM results were then compared to the ones obtained by exploiting the velocity response function of the system. It is found that, instead of the MDSM, the velocity response function can be used to obtain the effective friction expression, facilitating so the interpretation of the vibration-induced effects on the averaged friction force and avoiding the cumbersome mathematical steps needed for the extended MDSM. An equivalence was also shown between the aforementioned results and the alternative rationale used by Matunaga, Storck and coworkers and Kumar and Hutchings to compute the friction force reduction, based on the variation of friction force direction within one cycle of vibration.

The expression of the effective friction for a generic harmonic excitation is obtained for steady-state and continuous-slip motion. A procedure was proposed to define the boundaries of the transition from stick–slip to a continuous-slip regime, merging the rationale used by den Hartog and the velocity response function of a forced mass–spring system in contact with a moving belt. It is important to note that if the system is already in a slip regime (regardless of the presence of a moving belt), a friction reduction can be observed due to vibration. On the contrary, if the system is in a stick–slip regime at a specific excitation frequency as per den Hartog's stick–slip

plane, a belt velocity higher than the amplitude of the velocity response function (assuming sliding) will eliminate stick–slip, but no friction reduction will be observable according to the investigated system. It was also shown that the influence of the external loadings on friction depends on the combination of the loading phase, excitation frequency, system characteristics (mass, stiffness and damping values), and the value of the static friction coefficient. The choice of the normal contact force expression (including either inertia or damping-stiffness effects) also influences the results concerning the effective friction, and the velocity response function allows to shed light on the main mechanism (e.g. inertia or damping-stiffness) driving the contact normal force.

CRediT authorship contribution statement

E. Sulollari: Conceptualization, Methodology, Formal analysis, Investigation, Software, Original draft, Writing – review & editing, Visualization, Data curation. **K.N. van Dalen:** Writing – review & editing, Supervision. **A. Cabboi:** Conceptualization, Methodology, Writing – original draft, Writing – review & editing, Supervision.

Declaration of competing interest

The authors declare that they have no known competing financial interests or personal relationships that could have appeared to influence the work reported in this paper.

Data availability

Data will be made available on request.

Appendix

A.1. Extended MDSM for 2 DOF system; general harmonic loading

Separating the motions $[\mathbf{X}] = [X_1 \ X_2]^{\mathrm{T}}$ into the components $[\mathbf{Z}] = [Z_1 \ Z_2]^{\mathrm{T}}$ and $[\mathbf{\Phi}] = [\Phi_1 \ \Phi_2]^{\mathrm{T}}$, making use of the averaging operation and subtracting the equation of motion for $\mathbf{Z}$ from the total one, the equations of motion for the components in $\mathbf{\Phi}$, considering the arbitrary situation, are obtained

$$\begin{aligned}&\Omega_e\Phi_1'' + 2\dot{\Phi}_1' + \Omega_e^{-1}\ddot{\Phi}_1 + 2\beta_1\omega_1(\Phi_1' + \Omega_e^{-1}\dot{\Phi}_1) + \omega_1^2\Omega_e^{-1}\Phi_1 + \mu(-V_b + \Phi_1' + \Omega_e^{-1}\dot{\Phi}_1)(\omega_2^2\Omega_e^{-1}\Phi_2 + 2\beta_2\omega_2(\Phi_2' + \Omega_e^{-1}\dot{\Phi}_2)) \\ &+(\omega_2^2 Z_2 + 2\beta_2\omega_2\dot{Z}_2)\left(\mu(-V_b + \Phi_1' + \Omega_e^{-1}\dot{\Phi}_1) - \left\langle\mu(-V_b + \Phi_1' + \Omega_e^{-1}\dot{\Phi}_1)\right\rangle\right) = \alpha\Omega_e^2\sin(\Omega_e\tau)\end{aligned} \tag{A.1}$$

and

$$\Omega_e\Phi_2'' + 2\dot{\Phi}_2' + \Omega_e^{-1}\ddot{\Phi}_2 + 2\beta_2\omega_2(\Phi_2' + \Omega_e^{-1}\dot{\Phi}_2) + \omega_2^2\Omega_e^{-1}\Phi_2 = -\alpha\Omega_e^2\sin(\Omega_e\tau). \tag{A.2}$$

Note that Eqs. (A.1) and (A.2) are coupled, and the solution for Φ_1 is needed to find $\bar{\mu}(V_b)$. The solutions are sought in the form of the harmonic series presented below

$$\Phi_1 = B_{11}(\tau)\sin(\Omega_e\tau) + B_{12}(\tau)\cos(\Omega_e\tau) \tag{A.3}$$

$$\Phi_2 = B_{21}(\tau)\sin(\Omega_e\tau) + B_{22}(\tau)\cos(\Omega_e\tau). \tag{A.4}$$

Inserting Eqs. (A.3) and (A.4) into Eqs. (A.1) and (A.2) and gathering the coefficients of the involved harmonics $\sin(\Omega_e\tau)$ and $\cos(\Omega_e\tau)$, results in expressions for $\ddot{B}_{11}$, $\ddot{B}_{12}$, $\ddot{B}_{21}$ and $\ddot{B}_{22}$. After some mathematical manipulations, the equations of motion for $\mathbf{\Phi}$ can be solved analytically. All expressions of $B_{11}(\tau)$, $B_{12}(\tau)$, $B_{21}(\tau)$ and $B_{22}(\tau)$ approach to a constant value as τ increases reaching a steady-state condition. This behavior is shown in Fig. A.18 where all the plots are presented for the case of combined normal and tangential loading (2-DOF system).

A.2. Velocity response function for 2 DOF system; general harmonic loading

Here, the derivation of the velocity response function for the 2-DOF system is illustrated. For the 2DOF system, the assumed solution is

$$\mathbf{X} = \Im[\hat{\mathbf{X}}(\Omega_e)e^{\mathrm{i}\Omega_e t}], \tag{A.5}$$

since the external force is $F_{ext}(t) = \Im[\hat{F}_{ext}(\Omega_e)e^{\mathrm{i}\Omega_e t}]$. The frequency-dependant displacement response is then given by

$$\hat{\mathbf{X}}(\Omega_e) = \mathbf{H}(\Omega_e)\hat{\mathbf{F}}_{\mathbf{ext}}(\Omega_e), \tag{A.6}$$

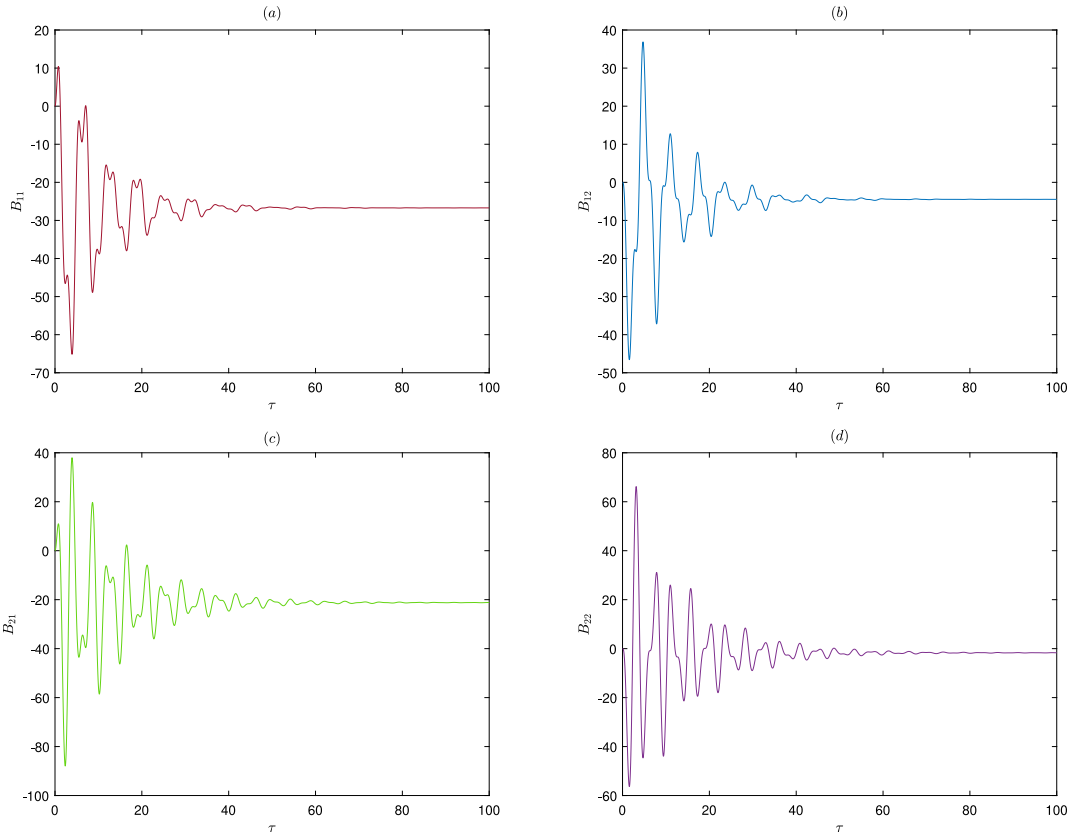

Fig. A.18. Transient and steady-state behavior of (a) $B_{11}(\tau)$ (red), (b) $B_{12}(\tau)$ (blue), (c) $B_{21}(\tau)$ (green) and (d) $B_{22}(\tau)$ (purple). $\Omega_e = 2$ and other parameters as in Fig. 11. (For interpretation of the references to color in this figure legend, the reader is referred to the web version of this article.)

where $\mathbf{H}(\Omega_e)$ is the transfer function, and its inverse reads as follows

$$\mathbf{H}(\Omega_e)^{-1} = \begin{bmatrix} -\Omega_e^2 + \mathrm{i}\Omega_e 2\beta_1\omega_1 + \omega_1^2 & \mu_s(\omega_2^2 + \mathrm{i}\Omega_e 2\beta_2\omega_2) \\ 0 & -\Omega_e^2 + \mathrm{i}\Omega_e 2\beta_2\omega_2 + \omega_2^2 \end{bmatrix}. \tag{A.7}$$

The displacement response function $\hat{X}_1(\Omega_e)$ becomes

$$\hat{X}_1(\Omega_e) = \frac{H_{22}(\Omega_e)\hat{F}_{1,ext}(\Omega_e) - H_{12}(\Omega_e)\hat{F}_{2,ext}(\Omega_e)}{H_{11}(\Omega_e)H_{22}(\Omega_e) - H_{12}(\Omega_e)H_{21}(\Omega_e)} = \frac{(-\Omega_e^2 + \mathrm{i}\Omega_e 2\beta_2\omega_2 + \omega_2^2)\hat{F}_{1,ext}(\Omega_e) - \mu_s(\omega_2^2 + \mathrm{i}\Omega_e 2\beta_2\omega_2)\hat{F}_{2,ext}(\Omega_e)}{|\mathbf{H}(\Omega_e)|}, \tag{A.8}$$

where $\hat{F}_{1,ext}(\Omega_e) = \alpha\Omega_e^2$, $\hat{F}_{2,ext}(\Omega_e) = -\alpha\Omega_e^2$ and $|\mathbf{H}(\Omega_e)|$ is the determinant of $\mathbf{H}(\Omega_e)$. The velocity response function can be easily found as

$$\hat{Y}_1(\Omega_e) = i\Omega_e\hat{X}_1(\Omega_e), \tag{A.9}$$

with the amplitude being

$$|\hat{Y}_1(\Omega_e)| = \sqrt{(\Im[\hat{Y}_1(\Omega_e)])^2 + (\Re[\hat{Y}_1(\Omega_e)])^2}. \tag{A.10}$$

References

[1] S.L. Ipri, H.H. Asada, Tuned dither for friction suppression during force-guided robotic assembly, in: Proc. 1995 IEEE/RSJ Int. Conf. on Intell. Robots and Systems. Human Robot Interaction and Cooperative Robots, vol. 1, 1995, pp. 310–315.

[2] A. Cabboi, T. Kamphuis, E. van Veldhuizen, M. Segeren, H. Hendrikse, Vibration-assisted decommissioning of a slip-joint: application to an offshore wind turbine, Eng. Struct. 76 (102931) (2021).

[3] A. Tsetas, A. Tsouvalas, S.S. Gómez, F. Pisanò, E. Kementzetzidis, T. Molenkamp, A.S.K. Elkadi, A.V. Metrikine, Gentle driving of piles (GDP) at a sandy site combining axial and torsional vibrations: Part I - installation tests, Ocean Eng. 270 (113453) (2023).

[4] W. Wu, C. Xu, C. Pan, Z. Huang, J. Zhou, P. Huang, Effect of vibration frequency on frictional resistance of brain tissue during vibration-assisted needle insertion, Med. Eng. Phys. 86 (2020) 35–40.

[5] J. Fu, Z. Ren, J. Bai, F. Qin, B. Li, The friction-reducing principle and application of the drill string with a hydro-oscillator, J. Petrol. Sci. Eng. 165 (2018) 453–461.

[6] K. Siegert, A. Möck, Wire drawing with ultrasonically oscillating dies, J. Mater Process. Technol. 60 (1–4) (1996) 657–660.
[7] A. Socoliuc, E. Gnecco, S. Maier, O. Pfeiffer, A. Baratoff, R. Bennewitz, M. E., Atomic-scale control of friction by actuation of nanometer-sized contacts., Science 313 (5784) (2006).
[8] D.J. Meyer, P. Wiertlewski, M. A., J.E. Colgate, Dynamics of ultrasonic and electrostatic friction modulation for rendering texture on haptic surfaces, IEEE Haptics Symp. (2014) 63–67.
[9] N.A. Muhammad, C.S. Wu, Ultrasonic vibration assisted friction stir welding of aluminium alloy and pure copper, J. Manuf. Process. 39 (2019) 114–127.
[10] H.D. Fridman, P. Levesque, Reduction of static friction by sonic vibrations, J. Appl. Phys. 30 (10) (1959) 1572–1575.
[11] D. Tolstoi, Significance of the normal degree of freedom and natural normal vibrations in contact friction, Wear 10 (3) (1967) 199–213.
[12] D.P. Hess, A. Soom, Normal vibrations and friction under harmonic loads: Part I–Hertzian contacts, J. Tribol. 113 (1) (1991) 80–86.
[13] D.P. Hess, A. Soom, Normal vibrations and friction under harmonic loads: Part II–rough planar contacts, J. Tribol. 113 (1) (1991) 87–92.
[14] D.P. Hess, A. Soom, C. Kim, Normal vibrations and friction at a Hertzian contact under random excitation: Theory and experiments, J. Sound Vib. 153 (3) (1992) 491–508.
[15] S. Matunaga, J. Onoda, New gravity compensation method by dither for low-g simulation, J. Spacecr. Rockets 32 (1995) 364–369.
[16] H. Storck, W. Littmann, J. Wallaschek, M. Mracek, The effect of friction reduction in presence of ultrasonic vibrations and its relevance to travelling wave ultrasonic motors, Ultrasonics 40 (1) (2002) 379–383.
[17] V. Kumar, I. Hutchings, Reduction of the sliding friction of metals by the application of longitudinal or transverse ultrasonic vibration, Tribol. Int. 37 (10) (2004) 833–840.
[18] M. Leus, P. Gutowski, Analysis of longitudinal tangential contact vibration effect on friction force using Coulomb and Dahl models, J. Theoret. Appl. Mech. 46 (1) (2008) 171–184.
[19] R.P. Dahl, Solid friction damping of mechanical vibrations, AIAA J. 14 (12) (1976) 1675–1682.
[20] K. Grudzinsky, R. Kostek, Influence of normal micro-vibrations in contact on sliding motion of solid body, J. Theoret. Appl. Mech. 43 (1) (2005) 37–49.
[21] V.L. Popov, J. Starcevic, A. Filippov, Influence of ultrasonic in-plane oscillations on static and sliding friction and intrinsic length scale of dry friction processes, Tribol. Lett. 39 (2010) 25–30.
[22] E. Teidelt, V. Popov, J. Starcevic, Influence of in-plane and out-of-plane ultrasonic oscillations on sliding friction, SAE Int. J. Passeng. Cars - Mech. Syst. 4 (3) (2011) 1387–1393.
[23] E. Teidelt, J. Starcevic, V. Popov, Influence of ultrasonic oscillation on static and sliding friction, Tribol. Lett. 48 (1) (2012) 51–62.
[24] M. Popov, V.L. Popov, N.V. Popov, Reduction of friction by normal oscillations. I. Influence of contact stiffness, Friction 5 (1) (2017) 45–55.
[25] X. Mao, V.L. Popov, J. Starcevic, M. Popov, Reduction of friction by normal oscillations. II. In-plane system dynamics, Friction 5 (2) (2017) 194–206.
[26] J.J. Thomsen, Using fast vibrations to quench friction-induced oscillations, J. Sound Vib. 228 (5) (1999) 1079–1102.
[27] I.I. Blekhman, Vibrational Mechanics – Nonlinear Dynamic Effects, General Approach, Applications, World Scientific, Singaopre, 2000.
[28] I.I. Blekhman, V.S. Sorokin, Effects produced by oscillations applied to nonlinear dynamic systems: a general approach and examples, Nonlinear Dynam. 83 (4) (2016) 2125–2141.
[29] V. Sorokin, Analysis of motion of inverted pendulum with vibrating suspension axis at low-frequency excitation as an illustration of a new approach for solving equations without explicit small parameter, Int. J. Non-Linear Mech. 63 (2014) 1–9.
[30] M.A. Michaux, A.A. Ferri, K. Cunefare, Effect of waveform on the effectiveness of tangential dither forces to cancel friction-induced oscillations, J. Sound Vib. 311 (3) (2008) 802–823.
[31] N. Hoffmann, N. Wagner, L. Gaul, Quenching mode-coupling friction-induced instability using high-frequency dither, J. Sound Vib. 279 (1) (2005) 471–480.
[32] S. Kapelke, W. Seemann, H. Hetzler, The effect of longitudinal high-frequency in-plane vibrations on a 1-DoF friction oscillator with compliant contact, Nonlinear Dynam. 88 (4) (2017) 3003–3015.
[33] S. Kapelke, W. Seemann, On the effect of longitudinal vibrations on dry friction: Modelling aspects and experimental investigations, Tribol. Lett. 66 (3) (2018).
[34] S. Shaw, On the dynamic response of a system with dry friction, J. Sound Vib. 108 (2) (1986) 305–325.
[35] U. Andreaus, P. Casini, Dynamics of friction oscillators excited by a moving base and/or driving force, J. Sound Vib. 245 (4) (2001) 685–699.
[36] K. Nakano, Two dimensionless parameters controlling the occurrence of stick-slip motion in a 1-DOF system with Coulomb friction, Tribol. Lett. 24 (2) (2006) 91–98.
[37] J.H. Dieterich, Modeling rock friction: 1. Experimental results and constitutive equations, J. Geophys. Res. 84 (1979) 2161–2168.
[38] C. Canudas deWit, H. Olsson, K. Astrom, P. Lischinsky, A new model for control of systems with friction, IEEE Trans. Automat. Control 40 (3) (1995) 419–425.
[39] V.S. Sorokin, J.J. Thomsen, Vibration suppression for strings with distributed loading using spatial cross-section modulation, J. Sound Vib. 335 (2015) 66–77.
[40] J. Den Hartog, LXXIII. Forced vibrations with combined viscous and Coulomb damping, Lond. Edinb. Dublin Philos. Mag. J. Sci. 9 (59) (1930) 801–817.